We are very grateful to the evaluations from the reviewers, which have allowed us to clarify and improve the manuscript. Below we addressed the reviewer comments, with the reviewer comments in black and our response in **blue**.

Reply for the referee comment#1

General Comments: HOMS are key players in atmospheric new particle formation and subsequent growth of secondary organic aerosol (SOA). They are formed through complex oxidation reaction networks and the process is called autoxidation. Due to the inherent complexity in gas-phase organic oxidation reactions combined with the multitude of uncertain and unknown branching pathways with minimal information of their number, efficiency and extent, describing HOM formation in atmospheric models is a formidable task. Hence, notwithstanding the importance of atmospheric autoxidation and direct aerosol precursor formation, describing it especially at the atmospheric scale remains an important barrier to overcome. Thus the work is novel, timely and aims to alleviate a persistent pain on the shoulders of the community. As such, it is certainly within scope of ACP and should be of interest to its readers. However, the inadequacies in reporting the work together with badly justified choice of parameters make the work untractable and not representative, and thus I can't propose publishing the work in ACP. I'll detail my concerns in the comments below.

Response: We sincerely thank the reviewer for their thoughtful and constructive assessment of our manuscript. We have carefully considered these comments and have undertaken substantial revisions to improve the clarity and robustness of our work. Specifically:

1. Reporting Improvements: We have thoroughly reorganized and expanded the methodology and results sections to more clearly and comprehensively describe the modeling framework and the improvements. In addition, we have incorporated schematic diagrams and flowcharts where appropriate to better guide the reader through the workflow and analytical steps.

2. Parameter Justification: We have provided more detailed explanations and references regarding the selection of key model parameters. Additionally, we explicitly discuss the associated uncertainties and their potential impact on the results through sensitivity analyses.

We hope that these revisions address the reviewer's concerns. A detailed account of all changes and specific responses is provided in the following section.

Major comments:

The two major issues with the current work are i) the apparent deliberate choice of parameters and ii) the insufficient documentation of the work. These are detailed separately below.

About the choice of parameters:

Major Comment#1: It seems the authors have chosen to use very high values for the crucial autoxidation parameters in several parts of the work, and thus it is not possible to assess the results at more realistic settings representing more atmospherically relevant conditions. The current study is probably closer to the maximum impact of monoterpenes on ambient HOM loads, though with the necessarily very reduced description of the oxidation chemistry in global models, no one could know today.

Importantly, the current work appears to almost completely hinge on the previous work of Xu et al., and uses its parameterizations without explaining the choices or what has actually been done. Whereas in Xu et al., there is a good discussion on the choice of parameters, here it is absent and the reader is left with very little information to understand the basis of the choices. It is also important to realize that the lower limit rate coefficients for autoxidation used here (i.e., around 0.1 s^-1 if I read it correctly) are already termed rapid rates in Xu et al., as they should be, as at around this rate the autoxidation is competitive in most atmospheric environments. In order to understand such a complex modelling work, it would be crucial to carefully detail the choice of parameters.

Related: How do you justify so high branching ratios to autoxidation, and why are they not described in the main text? Generally HOM yields have been found to lie between 0.1 and 7% of the VOC turnover.

Response: It is important to state that we agree with the reviewer that large uncertainties remain in the parameters, and we acknowledge this point in the manuscript. To address these uncertainties, we conduct sensitivity simulations, incorporating those related to key autoxidation parameters. Our current discussion of autoxidation parameter selection is presented in Text S1 of the Supporting Information. Given the importance of this topic, we have revised it in the updated manuscript the manuscript to include a more detailed explanation of the parameter choices in the main text, as outlined below:

> *To account for the H-shift chemistry of MT-RO_2 leading to HOM formation (i.e., autoxidation), the first-generation monoterpene-derived RO_2 (MT-RO_2), formed via reactions of monoterpenes (MT) with OH or O_3, is classified into two categories: MT-aRO_2 and MT-bRO_2 (Fig. 1). Both categories undergo standard bimolecular reactions, but only MT-bRO_2 species*

proceed through autoxidation. In contrast, MT-aRO₂ species (such as APINO₂, BPINO₂, LIMONO₂, and MYRCO₂, listed in Table S12) do not participate in autoxidation.

Relatively high branching ratios for the formation of MT-bRO₂ are adopted, based on the values used in Table S3 of Xu et al. (2022). Specifically, the branching ratio of MT-bRO₂ is 0.75 for monoterpene + OH reactions, and 0.08 for monoterpene + O₃ reactions (Fig. 1). These values fall within the ranges reported in previous studies. Literature-based yields for MT-bRO₂ range from 0.075 to 0.83 for OH-initiated reactions (Lee et al., 2023; Piletic and Kleindienst, 2022; Pye et al., 2019; Weber et al., 2020; Xu et al., 2019) and from 0 to 0.22 for O₃-initiated reactions (Ehn et al., 2014; Jokinen et al., 2015; Roldin et al., 2019; Berndt et al., 2016; Kurtén et al., 2015; Richters et al., 2016). The reaction rate constants for OH and O₃ oxidation of monoterpenes are the same as those used in the default mechanism (Table 3), and apply equally to the formation of both MT-aRO₂ and MT-bRO₂. This approach is fully consistent with the implementation in GEOS-Chem by Xu et al. (2022), who demonstrated that such simplification can reasonably reproduce the formation of HOMs and the fate of RO₂ radicals. Furthermore, studies by Roldin et al. (2019) and Weber et al. (2020) confirmed that using the same reaction rate for MT-bRO₂ and MT-aRO₂ also yields HOM concentrations that agree well with observations under forested conditions.

MT-bRO₂ are assumed to undergo one or multiple generations of autoxidation (Table 4). These reactions follow a temperature-dependent rate with an activation energy of 74.1 kJ/mol, consistent with previous studies (Lee et al., 2023; Möller et al., 2020; Pye et al., 2019; Roldin et al., 2019; Schervish and Donahue, 2020; Xu et al., 2019). The corresponding autoxidation rates are 0.27 s^{-1} at 283 K, 1.30 s^{-1} at 298 K, and 4.12 s^{-1} at 310 K. The yield of HOMs depends on both the autoxidation rate and the fraction of MT-RO₂ that undergoes autoxidation. To reflect the uncertainty associated with these parameters, this fraction is varied in both OH- and O₃-initiated pathways as part of sensitivity experiments. A detailed discussion of these tests is provided in Section 2.3.

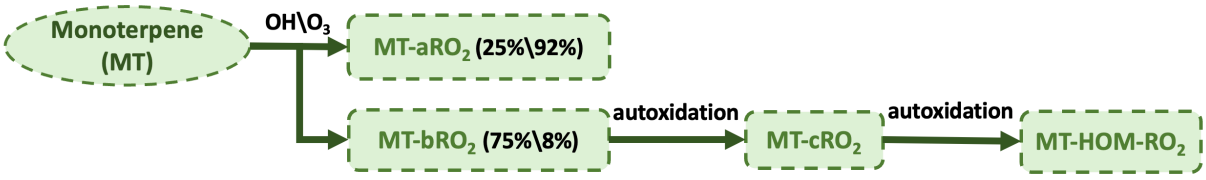

Figure 1. *Schematic of monoterpene (MT) oxidation and subsequent autoxidation pathways. MT reacts with OH or O₃ to form MT-aRO₂ or MT-bRO₂, with the latter undergoing autoxidation steps to yield HOMs. Branching ratios are shown for OH and O₃ pathways.*

Table 3. *Initial oxidation reactions of four representative monoterpenes (APIN, BPIN, LIMON, and MYRC) with OH and O_3, leading to the formation of MT-aRO_2 (non-autoxidizable) and MT-bRO_2 (autoxidizable). Detailed descriptions of the intermediate species are provided in Table S12.*

Index	*Reactions*	*Reaction rate*
1	*APIN[a] + OH → 0.25*MT-aRO_2 + 0.75*MT-bRO_2*	*1.34e-11*exp(410/T)*
2	*BPIN[a] + OH → 0.25*MT-aRO_2 + 0.75*MT-bRO_2*	*1.62e-11*exp(460/T)*
3	*LIMON[a] + OH → 0.25*MT-aRO_2 + 0.75*MT-bRO_2*	*3.41e-11*exp(470/T)*
4	*MYRC[a] + OH → 0.25*MT-aRO_2 + 0.75*MT-bRO_2*	*2.1e-10*
5	*APIN[a] + O_3 → 0.736*MT-aRO_2 + 0.064*MT-bRO_2 + 0.77*OH + 0.066*TERPA2O_2 + 0.22*H_2O_2 + 0.044*TERPA + 0.002*TERPACID + 0.034*TERPA2 + 0.17*HO_2 + 0.17*CO + 0.27*CH_2O + 0.054*TERPA2CO_3*	*1.34e-11*exp(410/T)*
6	*BPIN[a] + O_3 → 0.736*MT-aRO_2 + 0.064*MT-bRO_2 + 0.102*TERPK + 0.3*OH + 0.06*TERPA2CO_3 + 0.32*H_2O_2 + 0.038*BIGALK + 0.19*CO_2 + 0.81*CH_2O + 0.11*HMHP + 0.08*HCOOH*	*1.62e-11* exp(460/T)*
7	*LIMON[a] + O_3 → 0.736*MT-aRO_2 + 0.064*MT-bRO_2 + 0.66*OH + 0.132*TERPF1 + 0.33*CH_3CO_3 + 0.33*CH_2O + 0.066*TERPA3CO_3 + 0.33*H_2O_2 + 0.002*TERPACID*	*3.41e-11*exp(470/T)*
8	*MYRC[a] + O_3 → 0.736*MT-aRO_2 + 0.064*MT-bRO_2 + 0.2*TERPF2 + 0.63*OH + 0.63*HO_2 + 0.25*CH_3COCH_3 +0.39*CH_2O + 0.18*HYAC*	*2.1e-10*

[a] *APIN, BPIN, LIMON, and MYRC represent α-pinene, β-pinene, limonene, and myrcene, respectively.*

Table 4. *Autoxidation reactions of MT-bRO_2 leading to the formation of MT-cRO_2 and subsequently MT-HOM-RO_2.*

Index	*Reactions*	*Reaction rate*
9	*MT-bRO_2 → MT-cRO_2*	*9.8e12*exp(-8836/T)*
10	*MT-cRO_2 → MT-HOM-RO_2*	

The autoxidation rate from the "Fast" experiment in Xu et al. (2022) was adopted as the "control" rate in this study. The lowest autoxidation rate constant used in the simulations is not 0.1 s^{-1}, but rather 0.1 times the control rate. Accordingly, the Fast experiment applies a rate 10 times higher than the control. This is explicitly stated in line 186, as shown below:

"while two experiments (Fast and Slow) explore autoxidation rate extremes (×10 and ×0.1 of the Control rate)"

To assess the reliability of the autoxidation rates in the sensitivity experiments, the rates used in the Fast and Slow experiments were compared with those reported in previous chamber studies (Weber et al., 2019; Roldin et al., 2020). The results indicate that the Fast and Slow sensitivity experiments effectively cover the upper and lower bounds of the autoxidation rates observed in chamber experiments (see Figure and Table below).

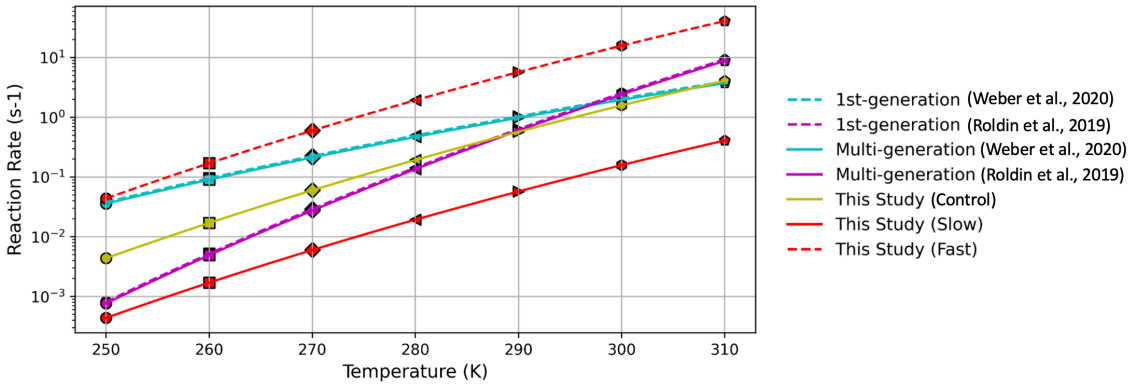

Figure. Comparison of temperature-dependent autoxidation rate used in this study (solid yellow, red, and dashed red lines for the Control, Slow, and Fast experiments, respectively) with first- and multi-generation autoxidation rates derived from previous chamber studies (Weber et al., 2019; Roldin et al., 2020; Xu et al., 2022).

Table. Description of the autoxidation rates used in different studies (Roldin et al., 2019; Weber et al., 2020).

Test Name	Reaction rate for generating	
	MT-cRO$_2$ (first-generation autoxidation products)	MT-HOM-RO$_2$ (multi-generation autoxidation products)
Weber et al. (2020)	1.009E9*exp(-6000/T)	9.500E8*exp(-6000/T)
Roldin et al. (2019)	7.768E17*exp(-12077/T)	7.311E17*exp(-12077/T)
This study	9.800E12*exp(-8836/T)	9.800E12*exp(-8836/T)

Our choice of high branching ratios for autoxidation has already been added in the main text (in abovemeionted response). It is important to note that the overall HOM yield and the branching ratio to autoxidation are not the same. The HOM yield is estimated by calculating the ratio of HOM concentration to monoterpene concentration in the atmosphere, which yields approximately 0.15% (see Figure below). This value falls within the 0.1% to 7% range mentioned by the reviewer.

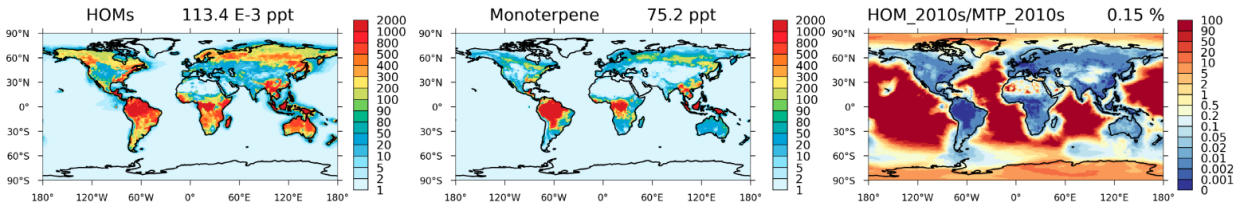

Figure. Annual mean surface concentrations of HOMs (left), monoterpenes (middle), and their mass concentration ratio (HOM/monoterpene, right) in the Control simulation for 2013. The global mean ratio is shown in the right panel.

Major Comment#2: "The reaction rate constants used are the same as those in the default monoterpene + OH/O3 reactions." So, what are they exactly and how reasonable is their use here? How does the lumping affect the diurnal cycles for example, as the actual rates depend on individual RO_2 concentrations.

Response: We are sorry for any confusion caused by the original sentence. To clarify, we have now included Table 3 in the revised manuscript, which explicitly lists the rate constants used for the monoterpene + OH/O_3 reactions (see the last response).

Currently, most models adopt similar parameterization schemes (the lumping effect). To make this clearer for readers, the following description will be added in the main text (the underlined content is newly added or modified):

> *The reaction rate constants for OH and O_3 oxidation of monoterpenes are the same as those used in the default mechanism (Table 3), and apply equally to the formation of both MT-aRO_2 and MT-bRO_2. This approach is fully consistent with the implementation in GEOS-Chem by Xu et al. (2022), who demonstrated that such simplification can reasonably reproduce the formation of HOMs and the fate of RO_2 radicals. Furthermore, studies by Roldin et al. (2019) and Weber et al. (2020) confirmed that using the same reaction rate for MT-bRO_2 and MT-aRO_2 also yields HOM concentrations that agree well with observations under forested conditions.*

Major Comment#3: I don't understand how the autoxidation rate can "critically regulate the formation pathways of accretion product generation by directly affecting the concentration of MT-HOM-RO2". Autoxidation only converts R'O2 to R''O2, so how would it affect total RO2 abundance? Are you modelling the RO2 + RO2 with increasing k as a function of the oxygen content?

Response: We appreciate the reviewer's thoughtful comment. Autoxidation does not directly alter the total RO_2 abundance, but instead redistributes the RO_2 species, thereby affecting the distribution of formation pathways for accretion products. To clarify this, we have revised the corresponding sentence in the manuscript (Line 272) as follows (The underlined content is newly added or modified):

> ~~*Autoxidation rates critically regulate the formation pathways of accretion product generation by directly affecting the concentration of MT-HOM-RO_2.*~~ *Autoxidation rates also influence the formation pathways of accretion products by affecting the distribution of peroxy radical intermediates. In the Slow experiment (×0.1 autoxidation rate), reduced MT-HOM-RO_2 production decreases its self-reaction contribution to C_{20} formation by 44% (from 27% to 15%) and cross-reactions contribution to C_{15} by 26% (from 50% to 37%). Conversely, the Fast experiment (with a 10-fold increase in the autoxidation rate) amplifies these contributions by 7% (C_{20}) and 4% (C_{15}), demonstrating a nonlinear response to rate changes.*

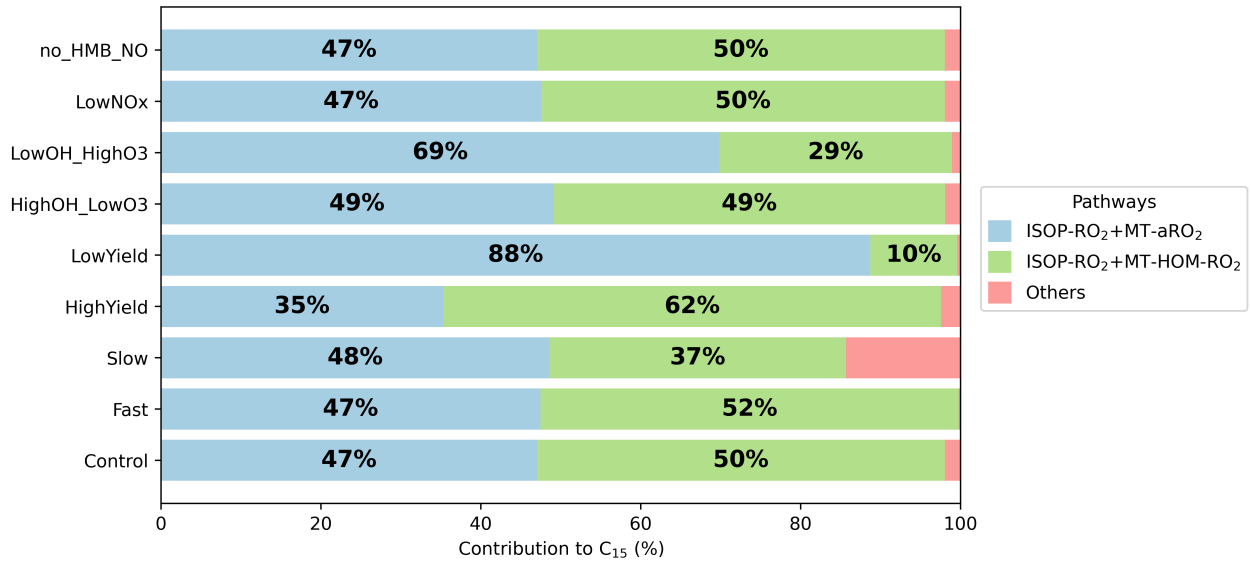

~~***Figure 5.***~~ ***Figure 7.*** *Contribution of different reaction pathways using different sensitivity tests (Table 8) to form C_{15} (HOMs containing 15 carbons). "ISOP-RO_2+MT-aRO_2" and "ISOP-RO_2+MT-HOM-RO_2" refer to Reactions 33-56 and 75-80 in Table 5. "Others" refers to other reactions forming C_{15} in Table 5.*

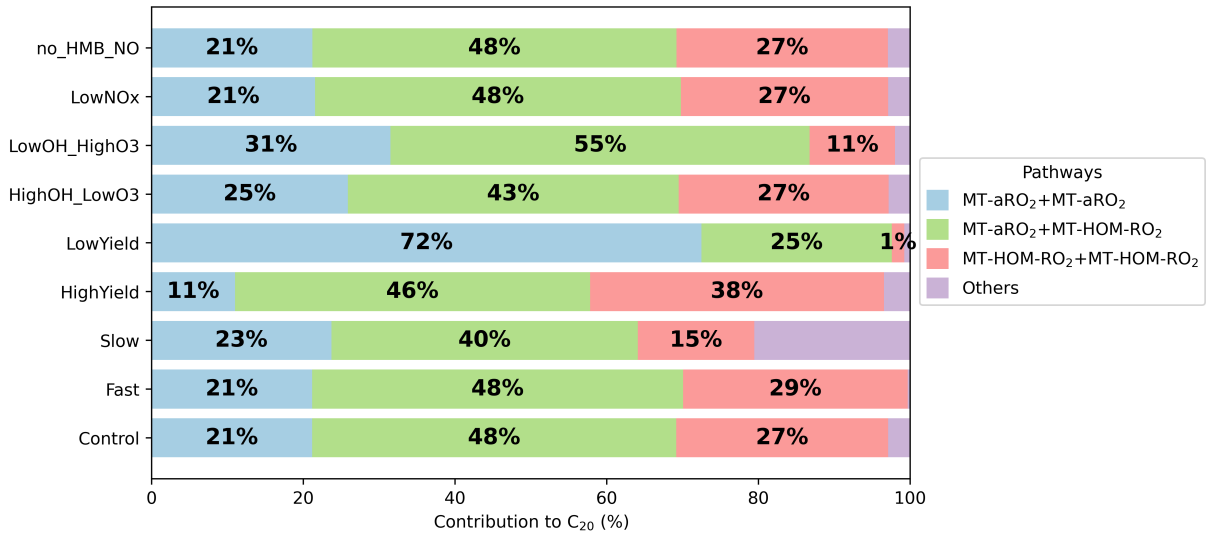

~~Figure 6.~~ ***Figure 8****. Contribution of different reaction pathways using different sensitivity tests (Table 8) to form C_{20} (HOMs containing 20 carbons). "MT-aRO₂+MT-aRO₂", "MT-aRO₂+MT-HOM-RO₂" and "MT-HOM-RO₂+MT-HOM-RO₂" refer to Reactions 11-20, 29-32 and 59 in Table 5. "others" refers to other reactions forming C_{20} in Table 5.*

Major Comment#4: Similarly this is a somewhat confusing statement "In addition, the reaction rates of autoxidation reactions remain highly uncertain, with different measurements in different chamber experiments ranging from 0.6 to 21 /s, differing by 1 to 2 orders of magnitude (Lee et al., 2023; Berndt et al., 2016; Moller et al., 2020)."

From this it appears that you are using too high autoxidation rates. Are the actual used rates described anywhere in the paper? 21 s^-1 is an exceptionally fast isomerization that outcompetes almost any RO2 loss process in almost any atmospheric environment. It is not representative number for general autoxidation in the atmosphere. It's also stated that autoxidation rates vary by 2 orders of magnitude, which is wrong. The meaningful variation is around 5 to 6 orders of magnitude (i.e., from around 10-4 to 100 s-1), but obviously the values can vary more than this.

Response: Sorry for the confusion caused by the original sentence. To clarify, we will add a new table (Table 3) and figure (Figure 1) in the revised manuscript to explicitly present the temperature-dependent autoxidation rate used in our simulations. We will also revise the relevant text for a clearer explanation, as follows:

> *MT-bRO₂ are assumed to undergo one or multiple generations of autoxidation (Table 4). These reactions follow a temperature-dependent rate with an activation energy of 74.1 kJ/mol, consistent with previous studies (Lee et al., 2023; Möller et al., 2020; Pye et al., 2019; Roldin et al., 2019; Schervish and Donahue, 2020; Xu et al., 2019). The corresponding autoxidation rate are 0.27 s^{-1} at 283 K, 1.30 s^{-1} at 298 K, and 4.12 s^{-1} at 310 K.*

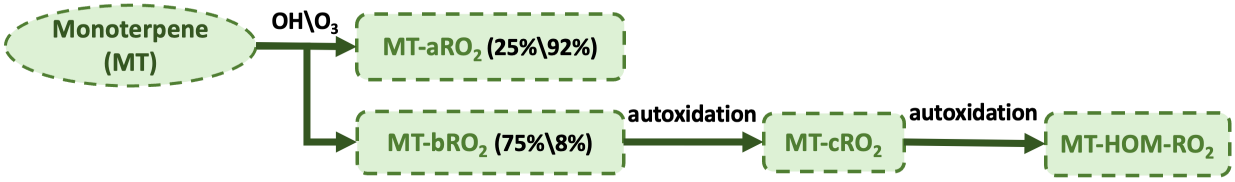

Figure 1. *Schematic of monoterpene (MT) oxidation and subsequent autoxidation pathways. MT reacts with OH or O_3 to form MT-aRO_2 or MT-bRO_2, with the latter undergoing successive autoxidation steps to yield MT-HOM-RO_2. Branching ratios are shown for OH and O_3 pathways.*

Table 4. *Autoxidation reactions of MT-bRO_2 leading to the formation of MT-cRO_2 and subsequently MT-HOM-RO_2.*

Index	*Reactions*	*Reaction rate*
9	*MT-bRO_2 → MT-cRO_2*	*9.8e12*exp(-8836/T)*
10	*MT-cRO_2 → MT-HOM-RO_2*	

We set the autoxidation rate in our sensitivity experiments to be 0.1 and 10 times the control value at a given temperature. However, when considering the full range of atmospheric temperatures in real general conditions, the resulting rate constants span approximately 5 orders of magnitude (from around 10^{-4} to 10 s^{-1}, see Figure and Table below). Moreover, the "Fast" and "Slow" experiments effectively capture the uncertainty range reported in previous chamber studies (Roldin et al., 2019; Weber et al., 2020).

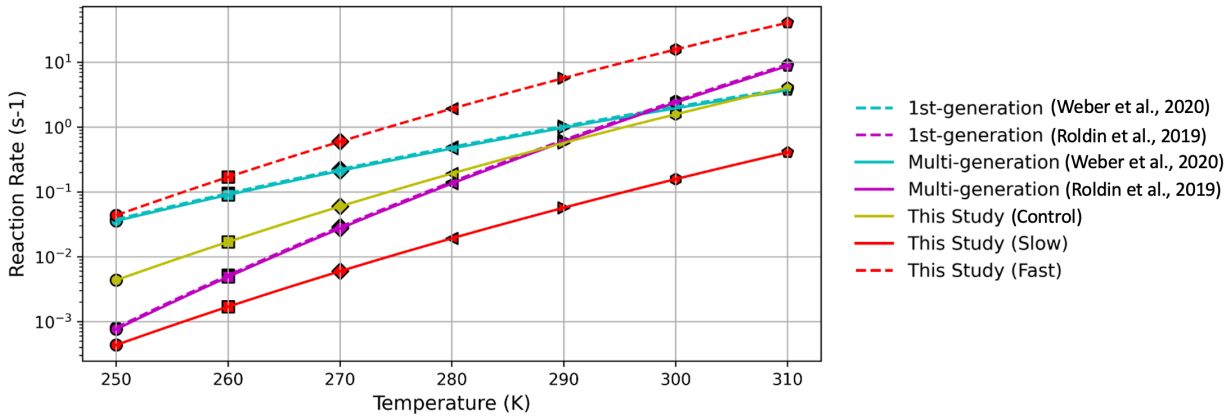

Figure. Comparison of temperature-dependent autoxidation rate used in this study (solid yellow, red, and dashed red lines for the Control, Slow, and Fast experiments, respectively) with first- and multi-generation autoxidation rates derived from previous chamber studies (Weber et al., 2019; Roldin et al., 2020; Xu et al., 2022).

Table. Description of the autoxidation rates used in different studies (Roldin et al., 2019; Weber et al., 2020).

Test Name	Reaction rate for generating	
	MT-cRO$_2$ (first-generation autoxidation products)	MT-HOM-RO$_2$ (multi-generation autoxidation products)
Weber et al. (2020)	1.009E9*exp(-6000/T)	9.500E8*exp(-6000/T)
Roldin et al. (2019)	7.768E17*exp(-12077/T)	7.311E17*exp(-12077/T)
This study	9.800E12*exp(-8836/T)	9.800E12*exp(-8836/T)

Major Comment#5: Moreover you say "The yields and reaction rates of the accretion products also vary by one to two orders of magnitude in different experimental measurements (Berndt et al., 2018; Zhao et al., 2018)."

Commonly RO2 + RO2 rates have been found to vary by over 6 orders of magnitude, which should be relevant for the RO2 +RO2 here as well. It appears that here all the RO2 + RO2 in the work have been given very high rate coefficients. Also the chosen CH3O2 rate coefficients seem strangely high (see e.g., https://doi.org/10.1016/j.atmosenv.2004.09.072)

Response: As shown in the Table below, the reactions involving CH_3O_2 (methylperoxy radicals) in our study are all between C_{10}-RO_2 and CH_3O_2. The reference you mentioned does not include reactions between CH_3O_2 and C_{10} or C_{10}-RO_2 species; it primarily focuses on reactions involving CH_3O_2 with smaller RO_2 species, such as C_5 compounds. Therefore, the rate coefficients we use fall outside the scope of that study and are chosen based on reaction types more relevant to the high-carbon RO_2 species considered in this work.

Table . MT-RO_2 reactions with methylperoxy radicals. Detailed descriptions of the intermediate species are provided in Table S12.

Reactions	Reaction rate
APINO$_2$ + CH$_3$O$_2$ → 0.05*MT-bRO$_2$ + 0.83*CH$_2$O + 0.133*TERPF1 + 0.399*TERPA + 0.19*TERPA3 + 0.1235*TERP1OOH + 0.17*CH$_3$OH + 0.1045*TERPK + 0.06*CH$_3$COCH$_3$ + 1.16*HO$_2$	2e-12
BPINO$_2$ + CH$_3$O$_2$ → 0.05*MT-bRO$_2$ + 1.4*CH$_2$O + 0.3515*TERPF1 + 0.304*TERPK + 1.5*HO$_2$ + 0.08*CH$_3$COCH$_3$ + 0.2945*TERPA3	2e-12
LIMONO$_2$ + CH$_3$O$_2$ → 0.05*MT-bRO$_2$ + 0.25*CH$_3$OH + 0.95*TERPF1 + 1.03*CH$_2$O + HO$_2$	2e-12
MYRCO$_2$ + CH$_3$O$_2$ → 0.05*MT-bRO$_2$ + 0.25*CH$_3$OH + 0.95*TERPF2 + 0.75*CH$_2$O + HO$_2$	2e-12
MT-bRO$_2$ \ MT-cRO$_2$ \ MT-HOM-RO$_2$ + CH$_3$O$_2$ → 0.15*CH$_3$OH + 0.85*CH$_2$O + 1.4*HO$_2$ + 0.7*HYDRALD + 0.7*CH$_3$COCH$_3$ + 0.15*C_{10}-ROH + 0.15*C_{10}-CBYL	3.56e-14* exp(708/T)

Based on a literature review, the uncertainty in reaction rate coefficients for highly oxygenated peroxy radicals to be within approximately two orders of magnitude. For shorter-chain RO_2 species, the uncertainty may be even greater, as noted in the reference you provided (https://doi.org/10.1016/j.atmosenv.2004.09.072). Accordingly, we have made the following revision in Line 67 (the underlined content is newly added or modified):

> *The yields and reaction rates of the accretion products also vary by one to two orders of magnitude in different experimental measurements (Berndt et al., 2018; Zhao et al., 2018; Roldin et al., 2019; Baker et al., 2024; Zhao et al., 2017; Molteni et al., 2019), with reported values ranging from 5 × 10^{-12} cm^3 s^{-1} (Baker et al., 2024) to 1 × 10^{-10} cm^3 s^{-1} (Berndt et al., 2018).*

The rate coefficients selected in this study (Table 5) fall within this reported range.

Table 5. *Summary of the self- and cross-reactions involving MT-RO_2 and ISOP-RO_2 peroxy radicals considered in this study. Detailed descriptions of the intermediate species are provided in Table S12.*

Index	*Reactions*	*Reaction rate*
11–20	*MT-aRO_2 + MT-aRO_2 → 0.893*C_{10}-CBYL + 0.29*C_{10}-ROH + 0.603*HO_2 + 1.34*HYDRALD + 0.067*MT-bRO_2 + 0.04* C_{20}*	*4.0e-11*
21–24	*MT-aRO_2 + MT-bRO_2 → 0.96*C10-CBYL + 0.29*C10-ROH + 0.67*HO2 + 1.34*HYDRALD + 0.04* C_{20}*	*4.0e-11*
25–28	*MT-aRO_2 + MT-cRO_2 → 0.96*C10-CBYL + 0.29*C10-ROH + 0.67*HO2 + 1.34*HYDRALD + 0.04* C_{20}*	*2.6e-10*
29–32	*MT-aRO_2 + MT-HOM-RO_2 → 0.96*C10-CBYL + 0.29*C10-ROH + 0.67*HO2 + 1.34*HYDRALD + 0.04* C_{20}*	*2.6e-10*
33–56	*MT-aRO_2 + ISOP-RO_2 → 0.4465*C10-CBYL + 0.145*C10-ROH + 0.145*ROH + 0.603*HO2+1.485*HYDRALD+0.0335*MT-bRO_2+ 0.04* C_{15}*	*2.0e-10*
57	*MT-bRO_2 + MT-bRO_2 → 0.96*C_{10}-CBYL + 0.29*C_{10}-ROH + 0.67*HO_2 + 1.34*HYDRALD + 0.04* C_{20}*	*4.0e-11*
58	*MT-cRO_2 + MT-cRO_2 → 0.96*C_{10}-CBYL + 0.29*C_{10}-ROH + 0.67*HO_2 + 1.34*HYDRALD + 0.04* C_{20}*	*2.6e-10*
59	*MT-HOM-RO_2 + MT-HOM-RO_2 → 0.96*C_{10}-CBYL + 0.29*C_{10}-ROH + 0.67*HO_2 + 1.34*HYDRALD + 0.04* C_{20}*	*2.6e-10*
60	*MT-bRO_2 + MT-cRO_2 → 0.96*C_{10}-CBYL + 0.29*C_{10}-ROH + 0.67*HO_2 + 1.34*HYDRALD + 0.04* C_{20}*	*2.6e-10*

61	*MT-bRO₂ + MT-HOM-RO₂ → 0.96*C₁₀-CBYL + 0.29*C₁₀-ROH + 0.67*HO₂ + 1.34*HYDRALD + 0.04* C₂₀*	*2.6e-10*
62	*MT-cRO₂ + MT-HOM-RO₂ → 0.96*C₁₀-CBYL + 0.29*C₁₀-ROH + 0.67*HO₂ + 1.34*HYDRALD + 0.04* C₂₀*	*2.6e-10*
63–68	*MT-bRO₂ + ISOP-RO₂ → 0.48*C₁₀-CBYL + 0.145*C₁₀-ROH + 0.145*ROH + 0.67*HO₂ + 1.485*HYDRALD + 0.04* C₁₅*	*2.0e-11*
69–74	*MT-cRO₂ + ISOP-RO₂ → 0.48*C₁₀-CBYL + 0.145*C₁₀-ROH + 0.145*ROH + 0.67*HO₂ + 1.485*HYDRALD + 0.04* C₁₅*	*4.0e-11*
75–80	*MT-HOM-RO₂ + ISOP-RO₂ → 0.48*C₁₀-CBYL + 0.145*C₁₀-ROH + 0.145*ROH + 0.67*HO₂ + 1.485*HYDRALD + 0.04* C₁₅*	*4.0e-11*

Major Comment#6: Related, you mention you have modelled self and cross reactions of the accretion products, but I suppose this is not what you meant. "while two experiments (Fast and Slow) explore autoxidation rate extremes (~10 and ~0.1 of the Control rate)." What is the actual Control Rate?

Response: Sorry for the confusion. What we modeled are the self- and cross-reactions of biogenic peroxy radicals that lead to the formation of accretion products, not the self- and cross-reactions of the accretion products themselves. To avoid any misunderstanding, we have revised the original sentence in the main text (the underlined content is newly added or modified):

> *HOM chemistry is also incorporated, including autoxidation reactions and self- and cross-reactions ~~for accretion products~~ of biogenic peroxy radicals forming accretion products, as described in Section 2.2.*

Additionally, revisions have been made to other areas that could be potentially ambiguous:

Line 67: "The yields and reaction rates of the accretion products" → "The yields and reaction rates to form accretion products"

Line 111 and Line 175: "self- and cross-reactions for accretion products" → "self- and cross-reactions to form accretion products"

Line 277: "fixed branching ratios for accretion products" → "fixed branching ratios to form accretion products"

As for the autoxidation rate in the Control experiment, the actual values used are now clarified in the revised manuscript in Table 4 (see details in the response to Major Comment 1).

Major Comment#7: "Building on this, we use sensitivity experiments (Table 2) to inform the uncertainties associated with the contribution of HOMs-SOA to MTSOA and total SOA". The Table 2 is hard to follow and thus it is not very clear what has been accomplished.

Response: Sorry for the confusion. Our main purpose here is to illustrate that several sensitivity experiments listed in Table 2, which primarily reflect chemical uncertainties related to HOMs, lead to variations in HOM concentrations. These changes subsequently affect HOMs-SOA concentrations and ultimately influence the contribution of HOMs-SOA to total SOA. To clarify, we have revised the sentence as follows (the underlined content is newly added or modified):

> *Building on this, we use the sensitivity experiments ~~(Table 2) to inform the uncertainties associated with the contribution of HOMs-SOA to MTSOA and total SOA~~ listed in Table 2 to examine how variations in HOM concentrations influence their contributions to MTSOA and total SOA.*

We believe that combining Table 2 with the description in Lines 178 to 194 (see below) provides a clear overview of the sensitivity experiments conducted.

> *The formation of monoterpene-derived HOMs involves two key uncertainties: (1) the branching ratios of autoxidation-capable peroxy radicals (MT-bRO$_2$) formed via OH- and O$_3$-initiated oxidation (Lee et al., 2023; Weber et al., 2020; Pye et al., 2019; Xu et al., 2019; Piletic and Kleindienst, 2022), and (2) the autoxidation rate of MT-bRO$_2$, which varies by over an order of magnitude in experimental studies (Berndt et al., 2018; Roldin et al., 2019; Weber et al., 2021). To systematically analyze these uncertainties, we conducted nine sensitivity experiments (Table 2). The Control experiment adopts the branching ratios from Xu et al. (2022) (MT-bRO$_2$: 75% for OH-initiated and 8% for O$_3$-initiated reactions), serving as a benchmark aligned with recent mechanistic frameworks. Four additional experiments (LowYield, HighYield, HighOH_LowO3, LowOH_HighO3) span the full parameter space of MT-bRO$_2$ branching ratios reported in literature (OH: 7.5–83%; O$_3$: 0.01–22%) (Saunders et al., 2003; Roldin et al., 2019; Rolletter et al., 2019), while two experiments (Fast and Slow) explore autoxidation rate extremes (×10 and ×0.1 of the Control rate). To isolate pathway-specific uncertainties in the formation of nitrate HOMs containing 10 carbons (C$_{10}$-ON) (Bianchi et al., 2019; Yan et al., 2016; Xu et al., 2022; Weber et al., 2020), we further test NO-mediated HOM formation (no_HMB_NO) (Reaction 110 in Table 6). Besides, in comparison with the SENEX and BAECC field campaigns, the simulated NO concentration in the Control experiment is overestimated by a factor of four (Figs. S1 and S2). Therefore, we multiplied the NO emissions by 0.2 in the LowNO experiment to assess the impact of anthropogenic NO on HOM concentration. These experiments collectively quantify how mechanistic uncertainties propagate to HOMs predictions, bridging gaps between chamber-derived parameters and global model applications.*

Table ~~2~~8. *Experiments used in this paper.*

Experiments	*OH branching ratio*	*O_3 branching ratio*	*Autoxidation rate*	*RO pathway*	*NO emissions*
Control	*75%*	*8%*	*K_{auto}* [a]	*√*	*default*
LowYield	*7.5%*	*0.01%*			
HighYield	*83%*	*22%*		*/* [b]	
HighOH_lowO3	*83%*	*0.01%*			
LowOH_HighO3	*7.5%*	*22%*			
Fast	*/*		*$10\times K_{auto}$*	*/*	
Slow			*$0.1\times K_{auto}$*		
no_HMB_NO		*/*		*X* [c]	*/*
~~LowNOx~~ LowNO		*/*			*default/5*

[a] *The specific values of K_{auto} are provided in Table 4*
[b] *The setting is the same as Control*
[c] *The yield of ~~b~~C_{10}-bNON is set to zero in the MT-HOM-RO_2 + NO reaction (reaction 110 in Table 6)*

About the documentation:

Major Comment#1: The minimum requirement of reporting a research work is that the work needs to be repeatable with the information given. Evenmore, the work has to be repeatable with the information given in the main text, and the supportting material is there to avoid unnecessary repetition and too big tables, etc. One should not need to look at the supporting material to comprehend what is presented in the main text. With the current level of documentation, I don't know how I could repeat the work.

Response: The schematic figure in the main text was intended only as a conceptual overview of the dominant oxidation steps, not as a full kinetic mechanism. We now recognize that this may have caused some confusion, and in response, we have provided additional schematic diagrams and summary tables to highlight the most important reactions (The full set of reactions can be found in the Tables S1–S9 and S12 of Supplementary Information). The specific additions are as follows:

2.2.2 Autoxidation

To account for the H-shift chemistry of MT-RO_2 leading to HOM formation (i.e., autoxidation), the first-generation monoterpene-derived RO_2 (MT-RO_2), formed via reactions of monoterpenes (MT) with OH or O_3, is classified into two categories: MT-aRO_2 and MT-bRO_2 (Fig. 1). Both categories undergo standard bimolecular reactions, but only MT-bRO_2 species proceed through autoxidation. In contrast, MT-aRO_2 species (such as $APINO_2$, $BPINO_2$, $LIMONO_2$, and $MYRCO_2$, listed in Table S12) do not participate in autoxidation.

Relatively high branching ratios for the formation of MT-bRO_2 are adopted, based on the values used in Table S3 of Xu et al. (2022). Specifically, the branching ratio of MT-bRO_2 is 0.75 for monoterpene + OH reactions, and 0.08 for monoterpene + O_3 reactions (Fig. 1). These values fall within the ranges reported in previous studies. Literature-based yields for MT-bRO_2 range from 0.075 to 0.83 for OH-initiated reactions (Lee et al., 2023; Piletic and Kleindienst, 2022; Pye et al., 2019; Weber et al., 2020; Xu et al., 2019) and from 0 to 0.22 for O_3-initiated reactions (Ehn et al., 2014; Jokinen et al., 2015; Roldin et al., 2019; Berndt et al., 2016; Kurtén et al., 2015; Richters et al., 2016). The reaction rate constants for OH and O_3 oxidation of monoterpenes are the same as those used in the default mechanism (Table 3), and apply equally to the formation of both MT-aRO_2 and MT-bRO_2. This approach is fully consistent with the implementation in GEOS-Chem by Xu et al. (2022), who demonstrated that such simplification can reasonably reproduce the formation of HOMs and the fate of RO_2 radicals. Furthermore, studies by Roldin et al. (2019) and Weber et al. (2020) confirmed that using the same reaction rate for MT-bRO_2 and MT-aRO_2 also yields HOM concentrations that agree well with observations under forested conditions.

MT-bRO₂ are assumed to undergo one or multiple generations of autoxidation (Table 4). These reactions follow a temperature-dependent rate with an activation energy of 74.1 kJ/mol, consistent with previous studies (Lee et al., 2023; Möller et al., 2020; Pye et al., 2019; Roldin et al., 2019; Schervish and Donahue, 2020; Xu et al., 2019). The corresponding autoxidation rate are 0.27 s^{-1} at 283 K, 1.30 s^{-1} at 298 K, and 4.12 s^{-1} at 310 K. The yield of HOMs depends on both the autoxidation rate and the fraction of MT-RO₂ that undergoes autoxidation. To reflect the uncertainty associated with these parameters, this fraction is varied in both OH- and O₃-initiated pathways as part of sensitivity experiments. A detailed discussion of these tests is provided in Section 2.3.

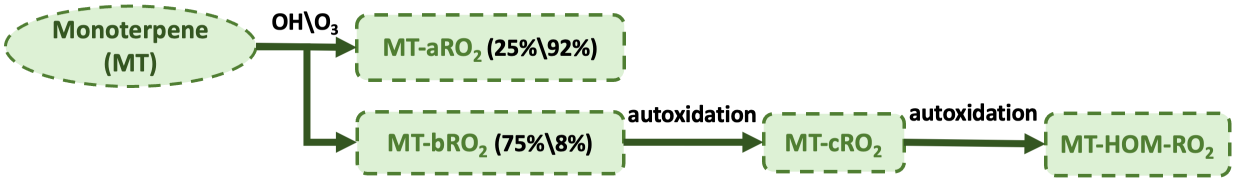

Figure 1. *Schematic of monoterpene (MT) oxidation and subsequent autoxidation pathways. MT reacts with OH or O₃ to form MT-aRO₂ or MT-bRO₂, with the latter undergoing autoxidation steps to yield HOMs. Branching ratios are shown for OH and O₃ pathways.*

Table 3. *Initial oxidation reactions of four representative monoterpenes (APIN, BPIN, LIMON, and MYRC) with OH and O₃, leading to the formation of MT-aRO₂ (non-autoxidizable) and MT-bRO₂ (autoxidizable). Detailed descriptions of the intermediate species are provided in Table S12.*

Index	Reactions	Reaction rate
1	$APIN^a + OH \rightarrow 0.25*MT\text{-}aRO_2 + 0.75*MT\text{-}bRO_2$	1.34e-11*exp(410/T)
2	$BPIN^a + OH \rightarrow 0.25*MT\text{-}aRO_2 + 0.75*MT\text{-}bRO_2$	1.62e-11*exp(460/T)
3	$LIMON^a + OH \rightarrow 0.25*MT\text{-}aRO_2 + 0.75*MT\text{-}bRO_2$	3.41e-11*exp(470/T)
4	$MYRC^a + OH \rightarrow 0.25*MT\text{-}aRO_2 + 0.75*MT\text{-}bRO_2$	2.1e-10
5	$APIN^a + O_3 \rightarrow 0.736*MT\text{-}aRO_2 + 0.064*MT\text{-}bRO_2 + 0.77*OH + 0.066*TERPA2O_2 + 0.22*H_2O_2 + 0.044*TERPA + 0.002*TERPACID + 0.034*TERPA2 + 0.17*HO_2 + 0.17*CO + 0.27*CH_2O + 0.054*TERPA2CO_3$	1.34e-11*exp(410/T)
6	$BPIN^a + O_3 \rightarrow 0.736*MT\text{-}aRO_2 + 0.064*MT\text{-}bRO_2 + 0.102*TERPK + 0.3*OH + 0.06*TERPA2CO_3 + 0.32*H_2O_2 + 0.038*BIGALK + 0.19*CO_2 + 0.81*CH_2O + 0.11*HMHP + 0.08*HCOOH$	1.62e-11* exp(460/T)

7	$LIMON^a + O_3 \rightarrow 0.736*MT\text{-}aRO_2 + 0.064*MT\text{-}bRO_2 + 0.66*OH + 0.132*TERPF1 + 0.33*CH_3CO_3 + 0.33*CH_2O + 0.066*TERPA3CO_3 + 0.33*H_2O_2 + 0.002*TERPACID$	3.41e-11*exp(470/T)
8	$MYRC^a + O_3 \rightarrow 0.736*MT\text{-}aRO_2 + 0.064*MT\text{-}bRO_2 + 0.2*TERPF2 + 0.63*OH + 0.63*HO_2 + 0.25*CH_3COCH_3 + 0.39*CH_2O + 0.18*HYAC$	2.1e-10

[a] *APIN, BPIN, LIMON, and MYRC represent α-pinene, β-pinene, limonene, and myrcene, respectively.*

Table 4. *Autoxidation reactions of $MT\text{-}bRO_2$ leading to the formation of $MT\text{-}cRO_2$ and subsequently $MT\text{-}HOM\text{-}RO_2$.*

Index	Reactions	Reaction rate
9	$MT\text{-}bRO_2 \rightarrow MT\text{-}cRO_2$	9.8e12*exp(-8836/T)
10	$MT\text{-}cRO_2 \rightarrow MT\text{-}HOM\text{-}RO_2$	

2.2.3 Self-Reactions and Cross-Reactions

Due to isomers of $MT\text{-}RO_2$ and $ISOP\text{-}RO_2$, self- and cross-reactions are included (Table 5), with three branches considered for the products. First, intermediate products are produced and are lumped as C_{10}-ROH and C_{10}-CBYL. Second, RO radicals are generated, which may produce HO_2 and C_{10}-CBYL or decompose into smaller compounds. Half of the RO radicals are assumed to decompose into smaller carbonyls. Third, accretion products (C_{15} and C_{20}) are produced. The branching ratios of the three pathways above are set as 0.29:0.67:0.04, respectively (Xu et al., 2022). However, for the self- and cross-reactions involving $MT\text{-}aRO_2$ ($APINO_2$, $BPINO_2$, $LIMONO_2$, and $MYRCO_2$ in Table S12) and $ISOP\text{-}RO_2$, a small fraction of RO radicals may undergo a unimolecular H-shift to form $MT\text{-}bRO_2$, with the branching ratio set to 0.05 (Xu et al., 2022). The fast reaction rate is applied here based on Table S4 in Xu et al. (2022).

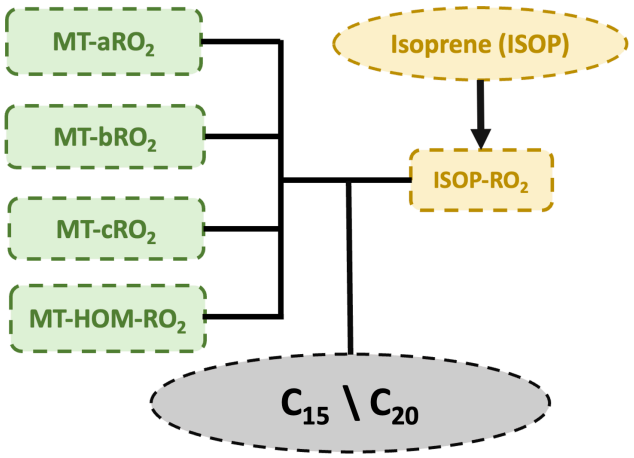

Figure 2. *Schematic illustration of self- and cross-reactions between $MT\text{-}RO_2$ and $ISOP\text{-}RO_2$ peroxy radicals.*

Table 5. *Summary of the self- and cross-reactions involving MT-RO_2 and ISOP-RO_2 peroxy radicals considered in this study. Detailed descriptions of the intermediate species are provided in Table S12.*

Index	*Reactions*	*Reaction rate*
11–20	*MT-aRO_2 + MT-aRO_2 → 0.893*C_{10}-CBYL + 0.29*C_{10}-ROH + 0.603*HO_2 + 1.34*HYDRALD + 0.067*MT-bRO_2 + 0.04* C_{20}*	*4.0e-11*
21–24	*MT-aRO_2 + MT-bRO_2 → 0.96*C10-CBYL + 0.29*C10-ROH + 0.67*HO2 + 1.34*HYDRALD + 0.04* C_{20}*	*4.0e-11*
25–28	*MT-aRO_2 + MT-cRO_2 → 0.96*C10-CBYL + 0.29*C10-ROH + 0.67*HO2 + 1.34*HYDRALD + 0.04* C_{20}*	*2.6e-10*
29–32	*MT-aRO_2 + MT-HOM-RO_2 → 0.96*C10-CBYL + 0.29*C10-ROH + 0.67*HO2 + 1.34*HYDRALD + 0.04* C_{20}*	*2.6e-10*
33–56	*MT-aRO_2 + ISOP-RO_2 → 0.4465*C10-CBYL + 0.145*C10-ROH + 0.145*ROH + 0.603*HO2+1.485*HYDRALD+0.0335*MT-bRO_2+ 0.04* C_{15}*	*2.0e-10*
57	*MT-bRO_2 + MT-bRO_2 → 0.96*C_{10}-CBYL + 0.29*C_{10}-ROH + 0.67*HO_2 + 1.34*HYDRALD + 0.04* C_{20}*	*4.0e-11*
58	*MT-cRO_2 + MT-cRO_2 → 0.96*C_{10}-CBYL + 0.29*C_{10}-ROH + 0.67*HO_2 + 1.34*HYDRALD + 0.04* C_{20}*	*2.6e-10*
59	*MT-HOM-RO_2 + MT-HOM-RO_2 → 0.96*C_{10}-CBYL + 0.29*C_{10}-ROH + 0.67*HO_2 + 1.34*HYDRALD + 0.04* C_{20}*	*2.6e-10*
60	*MT-bRO_2 + MT-cRO_2 → 0.96*C_{10}-CBYL + 0.29*C_{10}-ROH + 0.67*HO_2 + 1.34*HYDRALD + 0.04* C_{20}*	*2.6e-10*
61	*MT-bRO_2 + MT-HOM-RO_2 → 0.96*C_{10}-CBYL + 0.29*C_{10}-ROH + 0.67*HO_2 + 1.34*HYDRALD + 0.04* C_{20}*	*2.6e-10*
62	*MT-cRO_2 + MT-HOM-RO_2 → 0.96*C_{10}-CBYL + 0.29*C_{10}-ROH + 0.67*HO_2 + 1.34*HYDRALD + 0.04* C_{20}*	*2.6e-10*
63–68	*MT-bRO_2 + ISOP-RO_2 → 0.48*C_{10}-CBYL + 0.145*C_{10}-ROH + 0.145*ROH + 0.67*HO_2 + 1.485*HYDRALD + 0.04* C_{15}*	*2.0e-11*
69–74	*MT-cRO_2 + ISOP-RO_2 → 0.48*C_{10}-CBYL + 0.145*C_{10}-ROH + 0.145*ROH + 0.67*HO_2 + 1.485*HYDRALD + 0.04* C_{15}*	*4.0e-11*
75–80	*MT-HOM-RO_2 + ISOP-RO_2 → 0.48*C_{10}-CBYL + 0.145*C_{10}-ROH + 0.145*ROH + 0.67*HO_2 + 1.485*HYDRALD + 0.04* C_{15}*	*4.0e-11*

2.2.4 C_{10} HOMs formation

When MT-HOM-RO_2 are oxidized by HO_2, NO, or NO_3 (Fig. 3), three types of gas-phase C_{10} HOMs are formed: two types of C_{10} non-nitrate HOMs (C_{10}-aNON and C_{10}-bNON) and C_{10} nitrate HOMs (C_{10}-ON), as shown in Table 6. The rate constants used are the same as those for the MT-RO_2 + HO_2, NO, and NO_3 reactions in Xu et al. (2022).

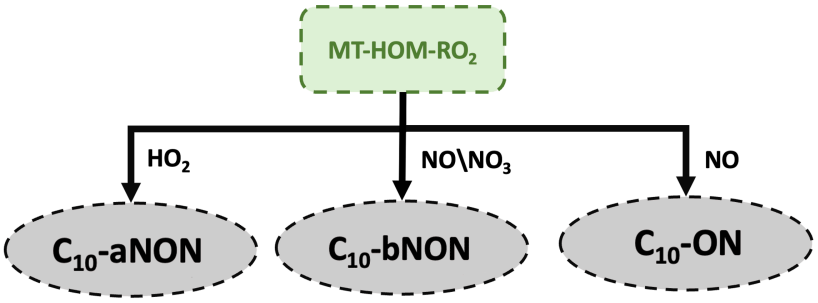

***Figure 3**. Schematic diagram illustrating the oxidation of MT-HOM-RO_2 by HO_2, NO, or NO_3, leading to the formation of three types of gas-phase C_{10}-HOMs.*

***Table 6.** C_{10} HOMs formation. Detailed descriptions of the intermediate species are provided in Table S12.*

Index	*Reactions*	*Reaction rate*
109	*MT-HOM-RO_2 + HO_2 → C_{10}-aNON + O_2*	*1.5e-11*
110	*MT-HOM-RO_2 + NO → 0.8*NO_2 + 0.8*HO_2 + 0.4* C_{10}-bNON + 0.8*HYDRALD + 0.2* C_{10}-ON*	*4.0e-12*
111	*MT-HOM-RO_2 + NO_3 → HO_2 + NO_2 + 0.5* C_{10}-ON + HYDRALD*	*1.2e-12*

Major Comment#2: You talk about "comprehensive HOMs chemical mechanism", but you are only showing a crude and rather ambiguous schematic of a handful of reaction steps that you apply for the whole pool of monoterpenes. This is really not a mechanism, which has a very specific meaning in the chemical literature. If there is no real base mechanism, then the involvement of NOx is even harder to understand. The NOx involvement seems to be particularly important for the current work, yet only the final results in the form of formed products seem to be represented and the mechanistic steps are not discussed. I would have really liked to see more discussion around the chemistry, which should be at the heart and sould of this work based on the title.

Figure 1 actually proposes a rather complex reaction chemistry but the text says you use 5 gaseous and 5 particle phase HOM in total. Where is this mismatch coming from?

Response: I agree that "comprehensive" is not appropriate, so we have used "a lumped HOMs mechanism" instead. While referring to it as a "comprehensive" chemical mechanism may not be

entirely accurate, we believe this constitutes a chemical mechanism, including reaction pathways, rate constants, and temperature dependence. These mechanisms (Figures 1-3 and Tables 3-6 in the last response) can be validated or reproduced in different models.

The influence of NO is first considered through the MOZART mechanism, and then further addressed by the scheme we implemented in this study. We did not consider the full impact of NO, but rather focused on the influence of NO on HOM formation. This is reflected in the termination reactions, which can lead to the formation of organic nitrates (C_{10}-ON) and non-organic nitrates (C_{10}-bNON) (Fig. 3). While we do not aim to propose a box-model mechanism here, we have expanded the discussion with more detailed sensitivity simulations around the chemistry.

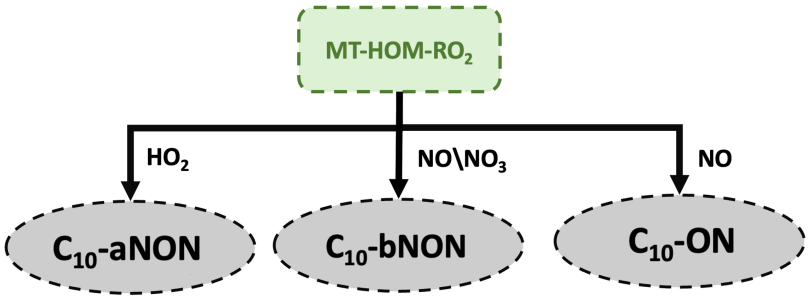

Figure 3. Schematic diagram illustrating the oxidation of MT-HOM-RO_2 by HO_2, NO, or NO_3, leading to the formation of three types of gas-phase C_{10} HOMs.

The uncertainties associated with NO are mainly discussed using two sensitivity experiments: no_HMB_NO (which eliminates NO-mediated C_{10}-bNON production due to large uncertainties in this reaction) (Bianchi et al., 2019; Yan et al., 2016; Xu et al., 2022; Weber et al., 2020) (Reaction 110 in Table 6) and LowNO (where NO emissions are reduced to 0.2 of the original value). The discussion of uncertainty in the formation pathway for both experiments can be found in lines 227 to 235 and lines 280 to 284 of the manuscript:

> *Compared to the dominant uncertainties in MT-bRO_2 branching ratios, the impacts of NO_x emissions and NO-mediated C_{10}-NON formation pathways are less significant, though they provide complementary insights into HOM chemistry. In the LowNO_x sensitivity experiment, total C_{10} concentrations decreased from 736 to 339 ng/m³ at the Centreville site (anthropogenically influenced) due to reduced NO_x emissions, with C_{10}-ON showing a more pronounced reduction (117 to 30 ng/m³) than C_{10}-NON (619 to 310 ng/m³), consistent with the NO-dependent formation of C_{10}-ON (Figs. 4 and 5). In contrast, at the SMEAR II site, total C_{10} remained nearly unchanged (141 to 142 ng/m³), reflecting minimal NO_x influence in the pristine region. Similarly, the no_HMB_NO experiment, which eliminates NO-mediated C_{10}-NON production, reduced C_{10}-NON concentrations by about 40% (619 to 398 ng/m³ at Centreville; 112 to 57 ng/m³ at SMEAR II) and improved agreement with observations (Figs. 4c and 5c).*

The LowNO and no_HMB_NO experiments show negligible changes in accretion pathways, as NO perturbations primarily alter terminal products (C_{10}-ON/C_{10}-bNON) rather than radical pools. This contrasts with Xu et al. (2022), who emphasized NO-driven HOM variability but did not isolate its limited impact on accretion chemistry.

Table 6. *C_{10} HOMs formation. Detailed descriptions of the intermediate species are provided in Table S12.*

Index	*Reactions*	*Reaction rate*
109	*MT-HOM-RO_2 + HO_2 → C_{10}-aNON + O_2*	*1.5e-11*
110	*MT-HOM-RO_2 + NO → 0.8*NO_2 + 0.8*HO_2 + 0.4* C_{10}-bNON + 0.8*HYDRALD + 0.2* C_{10}-ON*	*4.0e-12*
111	*MT-HOM-RO_2 + NO_3 → HO_2 + NO_2 + 0.5* C_{10}-ON + HYDRALD*	*1.2e-12*

The discussion on the uncertainty of the contribution of HOMs-SOA to total SOA in the two experiments can be found in the original manuscript from lines 324 to 326:

NO levels have a negligible effect (13% in LowNO experiment and 11% in no_HMB_NO experiment), which indicate that anthropogenic emissions do not significantly impact overall HOMs-SOA burdens.

The statement "use 5 gaseous and 5 particle-phase HOMs in total" refers to the five categories of final HOMs formed. After the partitioning of HOMs between the gas and particle phases, they generate 5 categories of SOA. There are numerous intermediate products in the entire reaction mechanism, all of which are summarized in Table S12. To avoid confusion, we will split Table 1.

The original Table 1 is as follows:

Table 1. *ΔH_{vap} at eight VBS bins. The first five bins are the traditional VBS bins and the last three bins are extended for HOMs mechanisms. aC_{10}-NON and bC_{10}-NON are the non-nitrate HOMs containing 10 carbons formed by HO_2 radical and NO pathways, respectively. C_{10}-ON are the nitrate HOMs containing 10 carbons. C_{15} and C_{20} are the HOMs containing 15 and 20 carbons, respectively.*

C^* ($\mu g/m^3$)	*SOAG*	*SOA*	*ΔH_{vap} (kJ/mol)*
1.0 x 10^{-2}	*SOAG0*	*soa1*	*153.0*
1.0 x 10^{-1}	*SOAG1*	*soa2*	*142.0*
1.0	*SOAG2*	*soa3*	*131.0*
1.0 x 10	*SOAG3*	*soa4*	*120.0*

1.0 x 10^{2}	*SOAG4*	*soa5*	*109.0*
	aC_{10}-NON (g) [a]	*aC_{10}-NON (a)* [b]	
1.0 x 10^{-3}	*bC_{10}-NON (g)* [a]	*bC_{10}-NON (a)* [b]	*164.0*
	C_{10}-ON (g) [a]	*C_{10}-ON (a)* [b]	
1.0 x 10^{-5}	*C_{15} (g)* [a]	*C_{15} (a)* [b]	*186.0*
1.0 x 10^{-9}	*C_{20} (g)* [a]	*C_{20} (a)* [b]	*230.0*

[a] Gas-phase HOMs, corresponding to SOAGhma, SOAGhmb, SOAGhmn, SOAGac15, and SOAGac20 in the model (Table S12).
[b] Particle-phase HOMs, corresponding to soahma, soahmb, soahmn, soaac15, and soaac20 in the model (Table S12).

The Table 1 will be revised as follows:

Table 1. *The saturated vapor concentration (C*) and vaporization enthalpies (ΔH_{vap}) of SOAG (SOA precursor gas) at the traditional VBS bins.*

C^* ($\mu g/m^3$)	*SOAG*	*ΔH_{vap} (kJ/mol)*
1.0 x 10^{-2}	*SOAG0*	*153.0*
1.0 x 10^{-1}	*SOAG1*	*142.0*
1.0	*SOAG2*	*131.0*
1.0 x 10	*SOAG3*	*120.0*
1.0 x 10^{2}	*SOAG4*	*109.0*

Also, we added a new Table 2 to characterize the newly generated HOMs:

Table 2*. The saturated vapor concentration (C*) and vaporization enthalpies (ΔH_{vap}) of HOMs.*

C^* ($\mu g/m^3$)	*ΔH_{vap} (kJ/mol)*	*Short Name*
1.0 x 10^{-3}	*164.0*	*C_{10}-aNON*
		C_{10}-bNON
		C_{10}-ON
1.0 x 10^{-5}	*186.0*	*C_{15}*
1.0 x 10^{-9}	*230.0*	*C_{20}*

Major Comment#3: Please use actual molecular compositions and not symbolic language. "TERP1OOH" is hardly a chemical name.

Response: Thank you for your valuable comment. It is not feasible for us to use actual molecular compositions throughout the manuscript because many intermediate products share identical molecular formulas, which would make it difficult to distinguish them in the reaction schemes (see Table S12 for details). Therefore, we have compiled Table S12 to list the molecular formulas and provide clear descriptions for all intermediate species. In addition, we have added the note "*Detailed descriptions of the intermediate species are provided in Table S12*" to the caption of each table presenting chemical reactions.

Major Comment#4: The photolysis assumptions. You say that photolysis of accretion products is not considered, but based on first principles they should be even more photosensitive as they contain the parent compound cromophores together with the added peroxide bond. Right? Or do you expect the HOM photochemistry to change considerably by addition of the peroxide bond? Also, shouldn't the photolysis frequency go down with the secondary particle size (i.e., shielding) or not? It is also unclear to me that where do you base the particle phase photolysis frequency that is as high as 1/60 of the jNO2?

Response: The reason for assuming either 1/60 of the j_{NO_2} or no photolysis for accretion products is explained in the main text, lines 167 to 169 (as shown below):

> *The gas-phase HOMs will undergo gas-particle partitioning to form particle-phase HOMs (Table 1 and Eq. (1)). Particle-phase C10 will be photolyzed (1.7% of the NO_2 photolysis frequency, Table S8), but the accretion products will not, due to large uncertainties (Zawadowicz et al., 2020; Xu et al., 2022).*

In our original simulations, we did not consider the decrease in photolysis frequency with increasing particle size (due to shielding effects). Although a previous study (Murphy et al., 2023) suggested that the addition of peroxide bonds may make compounds more susceptible to photolysis, there is currently no reliable chamber experiment providing an accurate photolysis rate for accretion products. Given the large uncertainty associated with this process, we added a sensitivity test in which accretion products are assumed to photolyze at the same rate as particle-phase C_{10} HOMs (i.e., 1.7% of the NO_2 photolysis rate). We have also included a corresponding explanation in the Section 5 (Conclusion) of the main text (see below) to help readers better understand the potential impact of this uncertainty on the simulation results.

> *To assess the potential influence of photolysis uncertainties, we performed a sensitivity experiment assuming that accretion products photolyze at the same rate as particle-phase C_{10} HOMs (i.e., 1.7% of the NO_2 photolysis rate). While the impact on smaller species such as*

C_{10}-ON and C_{10}-NON was negligible (<0.1%), substantial reductions were observed for C_{15} and C_{20} accretion products (75.2% and 68.1%, respectively) (Fig. S6). Overall, the total HOMs-SOA decreased by approximately 25.3% globally, highlighting that assumptions about photolysis rates can significantly affect model estimates of HOMs-SOA.

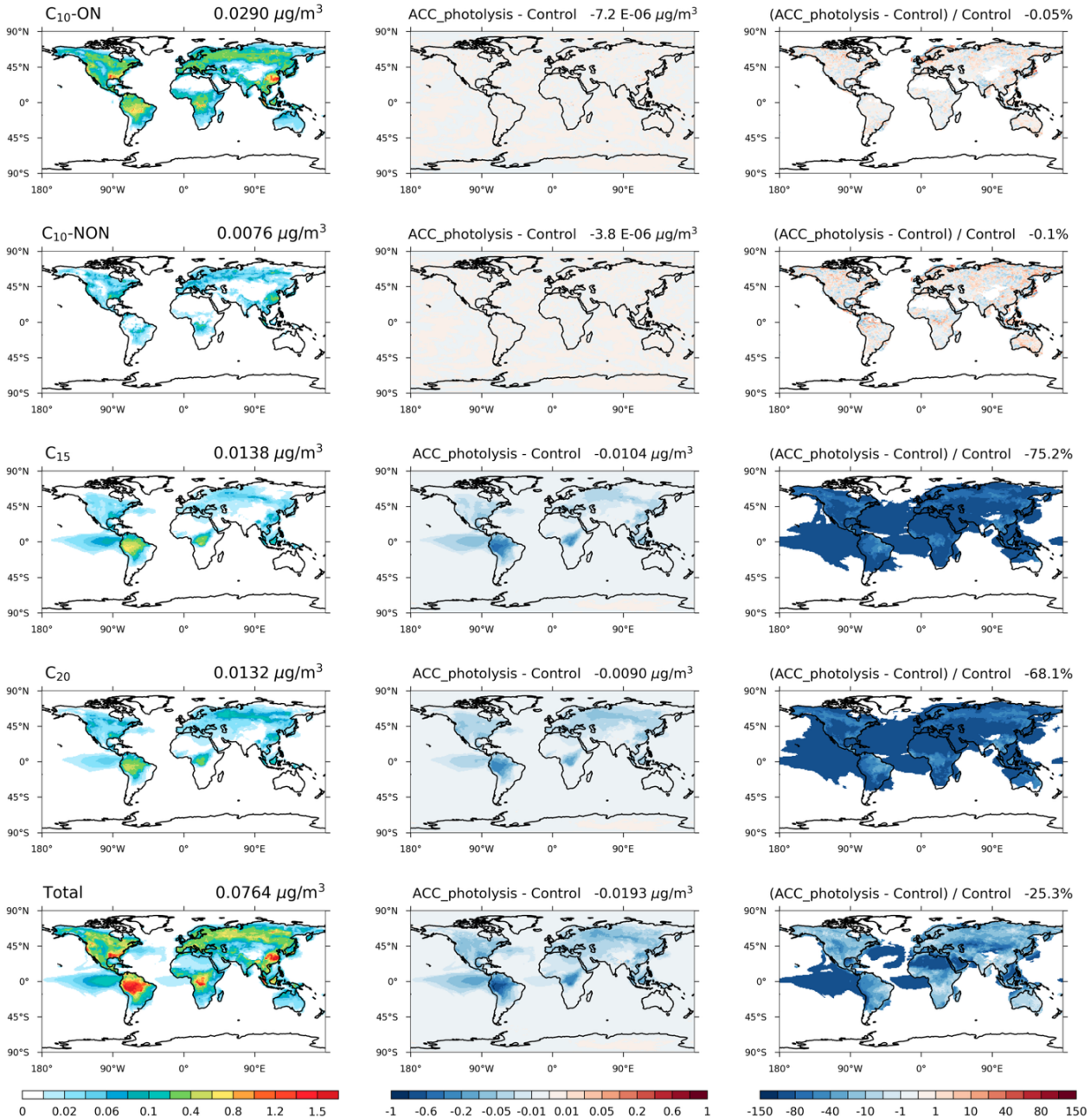

Figure S6. *Global distributions of particle-phase HOMs in the control simulation (left column), the absolute changes due to accretion product photolysis (ACC_photolysis - Control; middle column), and the relative changes (right column). Each row represents a specific HOM category: C_{10}-ON, C_{10}-NON, C_{15}, C_{20}, and the total.*

Major Comment#5: Unclear how the species would react together in Figure 1. Also, in each and every Figure you should explain all the names and symbols used. As an example, the Figure 2 is terribly hard to understood with the details given and one is left pondering about the numbers in them.

Response: Thank you for your comment. We have split Figure 1 into several smaller panels and added new textual descriptions and chemical reaction equations for each subfigure (see our response to Comment 1 for details). We apologize for the lack of clarity in the captions for Figures 2 and 3. We will revise both captions to more clearly convey the intended information. The underlined content in the revised captions indicates newly added or modified text (the underlined content is newly added or modified):

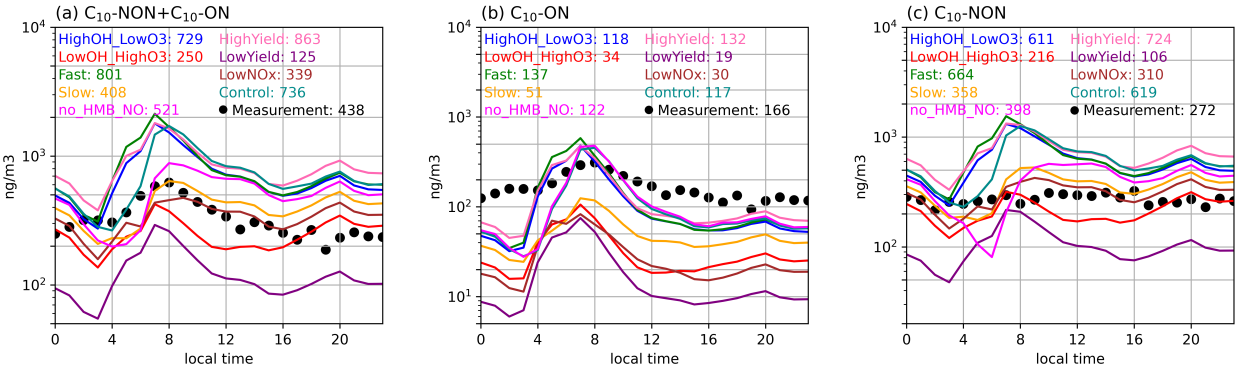

~~Figure 2.~~ Figure 4. *~~The diurnal cycle of observed (dots) surface and simulations (solid lines) total C_{10} (C_{10}-ON+ C_{10}-NON) (a), C_{10}-ON (b) and C_{10}-NON (c) concentrations (unit: ng/m^3) at the Centreville site during the SENEX campaign. The simulated surface C_{10} (C_{10}-ON and C_{10}-NON) concentrations at the closest grid to the Centreville site are used from simulations (solid lines). The simulated C_{10} at two sites are scaled by the ratios of the observed monoterpene concentrations to the simulated monoterpene concentrations (R_{MT}; Figure S1a and S2a). The Normalized Mean Bias (NMB), Correlation Coefficient (R), and Root Mean Square Error (RMSE) values of C_{10} comparing with observation are shown in Table S13. The C_{10}, C_{10}-NON and C_{10}-ON concentrations are the sum of gas-phase and particle-phase concentrations.~~* *Diurnal variations of observed (dots) and simulated (solid lines) surface concentrations of (a) total C_{10} (C_{10}-aON + C_{10}-bON + C_{10}-NON), (b) C_{10}-aON + C_{10}-bON, and (c) C_{10}-NON at the Centreville site. Simulations are scaled by the observed-to-simulated monoterpene ratios (see Figures S1a and S2a). All concentrations (ng/m^3) include both gas and particle phases. Numbers shown represent daily mean values. Sensitivity experiment information is provided in Table 8. Model performance metrics (NMB, R, RMSE) are provided in Table S13.*

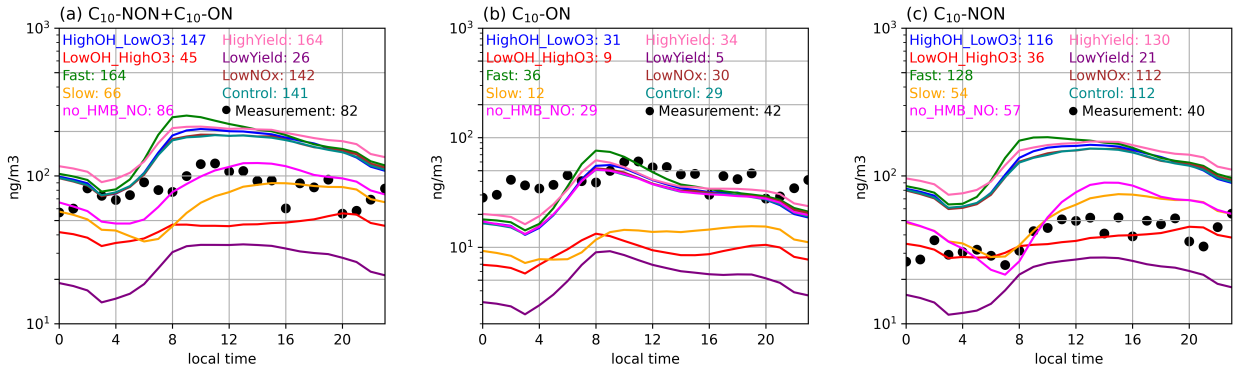

~~***Figure 3.***~~ ***Figure 5.*** ~~*The diurnal cycle of observed (dots) surface C_{10} (C_{10}-ON+ C_{10}-NON) (a), C_{10}-ON (b) and C_{10}-NON (c) concentrations (unit: ng/m^3) the SMEAR II sites during the BAECC campaign. The simulated surface C_{10} (C_{10}-ON and C_{10}-NON) concentrations at the closest grid to the SMEAR II site are used from different simulations (solid lines). The simulated C_{10} at two sites are scaled by the ratios of the observed monoterpene concentrations to the simulated monoterpene concentrations (R_{MT}, Figure S1a and S2a). The Normalized Mean Bias (NMB), Correlation Coefficient (R), and Root Mean Square Error (RMSE) values of C_{10} comparing with observation are shown in Table S13. The C_{10}, C_{10}-NON and C_{10}-ON concentrations are the sum of gas-phase and particle-phase concentrations.*~~ *Diurnal variations of observed (dots) and simulated (solid lines) surface concentrations of (a) total C_{10} (C_{10}-aON + C_{10}-bON + C_{10}-NON), (b) C_{10}-aON + C_{10}-bON, and (c) C_{10}-NON at the SMEAR II site. Simulations are scaled by the observed-to-simulated monoterpene ratios (see Figures S1a and S2a). All concentrations (ng/m³) include both gas and particle phases. Numbers shown represent daily mean values. Sensitivity experiment information is provided in Table 8. Model performance metrics (NMB, R, RMSE) are provided in Table S13.*

Major Comment#6: Explain all the terms and symbols in Table and Figure captions. For example, can't understand Table 2.

Response: Thank you for pointing this out. We have carefully revised all table and figure captions to clearly define all terms, abbreviations, and symbols used (see our response to Comment 1 for details). Regarding the description of Table 2, it is mentioned in the main text from lines 178 to 194 (the underlined content is newly added or modified):

> *The formation of monoterpene-derived HOMs involves two key uncertainties: (1) the branching ratios of autoxidation-capable peroxy radicals (MT-bRO$_2$) formed via OH- and O$_3$-initiated oxidation (Lee et al., 2023; Weber et al., 2020; Pye et al., 2019; Xu et al., 2019; Piletic and Kleindienst, 2022), and (2) the autoxidation rate of MT-bRO$_2$, which varies by over an order of magnitude in experimental studies (Berndt et al., 2018; Roldin et al., 2019; Weber et al., 2021). To systematically analyze these uncertainties, we conducted nine sensitivity experiments (Table 2). The Control experiment adopts the branching ratios from Xu et al. (2022) (MT-bRO$_2$: 75% for OH-initiated and 8% for O$_3$-initiated reactions), serving as a benchmark aligned with recent mechanistic frameworks. Four additional experiments (LowYield, HighYield, HighOH_LowO3, LowOH_HighO3) span the full parameter space of*

MT-bRO₂ branching ratios reported in literature (OH: 7.5–83%; O₃: 0.01–22%) (Saunders et al., 2003; Roldin et al., 2019; Rolletter et al., 2019), while two experiments (Fast and Slow) explore autoxidation rate extremes (×10 and ×0.1 of the Control rate). To isolate pathway-specific uncertainties in the formation of nitrate HOMs containing 10 carbons (C_{10}-ON) (Bianchi et al., 2019; Yan et al., 2016; Xu et al., 2022; Weber et al., 2020), we further test NO-mediated HOM formation (no_HMB_NO) (Reaction 110 in Table 6). Besides, in comparison with the SENEX and BAECC field campaigns, the simulated NO concentration in the Control experiment is overestimated by a factor of four (Figs. S1 and S2). Therefore, we multiplied the NO_x emissions by 0.2 in the LowNO_x experiment to assess the impact of anthropogenic NO_x on HOM concentration. ~~These experiments collectively quantify how mechanistic uncertainties propagate to HOMs predictions, bridging gaps between chamber-derived parameters and global model applications.~~ These experiments help quantify how uncertainties in chemical mechanisms affect HOM concentrations in global models.

Less Major Comments

Comment#1: "In the LowNOx sensitivity experiment, total C10 concentrations decreased from 736 to 339 ng/m3 at the Centreville site (anthropogenically influenced) due to reduced NOx emissions, with C10-ON showing a more pronounced reduction (117 to 30 ng/m3) than C10-NON (619 to 310 ng/m3), consistent with the NO-dependent formation of C10-ON (Figs. 2 and 3)." There seems to be a bad disconnect here as the C10 How does the C10 concentrations decrease with reducing NOx? Is the NO involvement through RO formation taken into consideration.

Response: NO acts as a reactant and is involved in the formation of both C_{10}-ON and C_{10}-NON (as shown in Table 6 and Fig. 3). When NO concentrations decrease, the production rates of both species decrease, which in turn affects their concentrations. The main point here is that C_{10}-ON is more sensitive to changes in NO concentrations compared to C_{10}-NON. This is because C_{10}-ON formation is primarily driven by NO (Fig. 3), while C_{10}-NON can also be formed through other oxidants, such as HO_2 and NO_3.

To avoid misunderstanding, we have revised the sentence in lines 228 to 231 (the underlined content is newly added or modified):

> *In the ~~LowNOx~~ LowNO sensitivity experiment, total C_{10} concentrations decreased from 736 to 339 ng/m³ at the Centreville site (anthropogenically influenced) due to reduced ~~NO_x~~ NO emissions, with C_{10}-ON showing a more pronounced reduction (117 to 30 ng/m³) than C_{10}-NON (619 to 310 ng/m³), consistent with the NO-dependent formation of C_{10}-ON (~~Figs. 2 and 3~~ Fig. 3 and Table 6).*

Additionally, the name of the sensitivity experiment has been changed throughout the manuscript from LowNOx to LowNO.

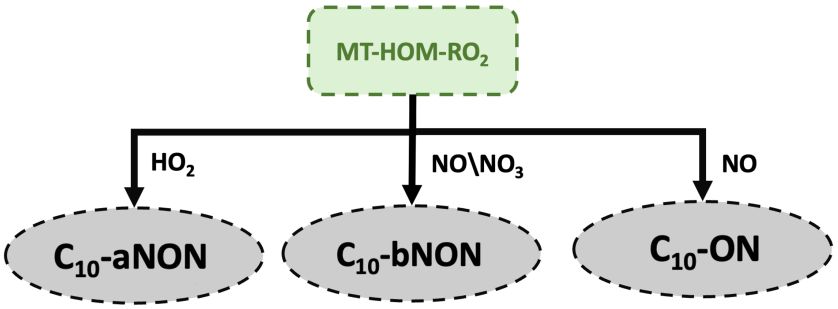

Figure 3. *Schematic diagram illustrating the oxidation of MT-HOM-RO_2 by HO_2, NO, or NO_3, leading to the formation of three types of gas-phase C_{10} HOMs.*

Table 6. *C_{10} HOMs formation. Detailed descriptions of the intermediate species are provided in Table S12.*

Index	*Reactions*	*Reaction rate*
109	*MT-HOM-RO_2 + HO_2 → C_{10}-aNON + O_2*	*1.5e-11*
110	*MT-HOM-RO_2 + NO → 0.8*NO_2 + 0.8*HO_2 + 0.4* C_{10}-bNON + 0.8*HYDRALD + 0.2* C_{10}-ON*	*4.0e-12*
111	*MT-HOM-RO_2 + NO_3 → HO_2 + NO_2 + 0.5* C_{10}-ON + HYDRALD*	*1.2e-12*

Comment#2: "The MT-RO2 formed by the oxidation of monoterpenes by NO_3 radicals are not considered in this study, as some studies report the branching ratio to be insignificant". This seems strange as several recent studies are finding NO3 oxidation far more important than has been previously thought. Perhaps you're confusing with the work of Kurtén et al., who explained that the one monoterpene that most people seem to concentrate do not have facile paths to HOM upon NO3 initiated oxidation (https://pubs.acs.org/doi/10.1021/acs.jpclett.7b01038), but it is unlikely that this result transfers to other monoterpene systems.

Response: Sorry for ignoring the role of NO_3-initiated oxidation pathways in our previous discussion. We have revised the manuscript in Lines 138 to 150 (the underlined content is newly added or modified):

> *The MT-RO_2 formed by the oxidation of monoterpenes by NO_3 radicals is not considered in this study, as some studies report that the branching ratio remains highly uncertain ~~to be insignificant~~ (Zhao et al., 2021; Nah et al., 2016; Yan et al., 2016; Roldin et al., 2019)~~, and the chemical process remains highly uncertain (Roldin et al., 2019)~~.*

Additionally, the following discussion has been added in Section 5 (Conclusion):

> *This study investigates the formation of HOMs from monoterpene oxidation in a global simulation, yet significant uncertainties remain in the representation of NO_3-initiated pathways. Recent studies suggest that NO_3-initiated HOM formation may be more important than previously thought, particularly under polluted nighttime conditions. Chamber experiments on α- and β-phellandrene oxidation by NO_3 have shown significant SOA and HOM production, with SOA yields reaching approximately 35% and 60%, respectively, accompanied by abundant HOM monomers and dimers (Harb et al., 2024). Furthermore, field observations from the southeastern United States indicate that NO_3 remains the dominant oxidant of monoterpenes at night, accounting for around 60% (observed) to 80% (modeled) of total monoterpene oxidation (Desai et al., 2024). These results highlight the potential importance of NO_3-initiated HOM formation in contributing to organic aerosol formation under polluted nighttime conditions. However, due to structural differences in monoterpenes,*

such as ring strain and double-bond position, HOM yields vary widely among different species (Dam et al., 2022; Draper et al., 2024) and are highly sensitive to ambient NO_x concentrations and humidity (Pasik et al., 2025; Li et al., 2022). The incomplete understanding of these mechanisms limits the accuracy of HOM predictions in models. Future research should combine field observations, laboratory constraints, and updated reaction schemes to reduce these uncertainties and improve global-scale modeling of nighttime organic aerosol formation.

Comment#3: It is unclear how you are using the field data here. Do you estimate the individual C10 species concentrations from the experimental data? Did you obtain the raw data from the authors, or how did you come up with the signals? What sort of calibration factors were used?

Response: HOM measurements in this study were obtained using a high-resolution time-of-flight chemical ionization mass spectrometer (HRToF-CIMS), following the approach of Lopez-Hilfiker et al. (2014) where available. For the definition of HOMs, we selected compounds with molecular formulas containing 10 carbon atoms and at least 7 oxygen atoms.

The signals originate from FIGAERO-HRToF-CIMS thermal desorption measurements, in which sampled aerosol compounds are desorbed via a temperature ramp and subsequently detected as ion signals by the HRToF-CIMS. For quantification, a formic acid sensitivity was applied as the calibration factor, with a typical value of ~10 counts per second (cps) per ppt, to convert ion signals to concentrations (Lopez-Hilfiker et al., 2014).

The data used in this study were obtained from publicly available repositories:
SOAS campaign:
https://csl.noaa.gov/groups/csl7/measurements/2013senex/Ground/DataDownload/

BAECC campaign: https://www.arm.gov/research/campaigns/amf2014baecc

SMEAR II dataset: https://smear.avaa.csc.fi/download

To improve readability and clarity for the reader, we have expanded Section 2.3 (Observations) to include additional details regarding the field campaigns. The updated Section 2.3 is provided below:

Data from two campaigns were used for comparison: the Southern Oxidant and Aerosol Study (SOAS) in the southeastern USA, and the Biogenic Aerosols – Effects on Clouds and Climate (BAECC) in Hyytiälä, Finland (Carlton et al., 2018; Martin et al., 2016; Petäjä et al., 2016) (Table 7). HOM measurements were obtained using high-resolution time-of-flight chemical ionization mass spectrometer (HRToF-CIMS) when available (Lopez-Hilfiker et al., 2014). For HOM measurements, molecular formulas of compounds containing 10 carbon atoms and at least 7 oxygen atoms were selected as HOMs. The compounds with one nitrate and without

nitrate were compared to the simulated C_{10}-aNON, C_{10}-bNON, and C_{10}-ON, respectively. In addition to HOMs, related species such as NO, O_3, monoterpenes, and isoprene were also compared when the data was available (Figs. S1 and S2). The primary HOM species identified in the SENEX (Southeast Nexus) and BAECC campaigns (Tables S15 and S16).

Table 7. *Field campaigns used in this paper*

Campaigns	*Dates*	*Locations*
SOAS (Warneke et al., 2016)	*2013.06.01–07.15*	*Centreville, Alabama, US (32.93°N, 87.13°W)*
BAECC (Petäjä et al., 2016)	*2014.04.11–06.03*	*Station for Measuring Ecosystem Atmosphere Relations (SMEAR II), Hyytiälä, Finland. (61.85°N，24.28°E）*

Table S15. *Molecular formulas of top 5 contributing HOM-ON and HOM-NON species (gas- and particle-phase) at Centreville, Alabama*

HOM-ON		***HOM-NON***	
Gas-phase	***Particle-phase***	***Gas-phase***	***Particle-phase***
C10H15O7N1	*C10H15O7N1*	*C10H14O7*	*C10H14O7*
C10H17O7N1	*C10H15O8N1*	*C10H12O7*	*C10H12O7*
C10H15O8N1	*C10H17O7N1*	*C10H22O8*	*C10H16O7*
C10H17O8N1	*C10H17O8N1*	*C10H22O7*	*C10H22O8*
C10H13O8N1	*C10H15O9N1*	*C10H16O7*	*C10H22O7*

Table S16. *Molecular formulas of top 5 contributing HOM-ON and HOM-NON species (gas- and particle-phase) at Hyytiälä, Finland*

HOM-ON		***HOM-NON***	
Gas-phase	***Particle-phase***	***Gas-phase***	***Particle-phase***
C10H15O7N1	*C10H15O8N1*	*C10H12O11*	*C10H14O7*
C10H15O8N1	*C10H15O7N1*	*C10H14O8*	*C10H22O9*
C10H17O7N1	*C10H17O7N1*	*C10H16O8*	*C10H22O7*
C10H13O7N1	*C10H17O8N1*	*C10H14O7*	*C10H22O8*

C10H17O8N1	*C10H15O9N1*	*C10H22O7*	*C10H16O7*

Comment#4: Related, I would like the authors to comment on the assumed volatility classes. How sure it is that the compounds assumed ELVOC, are actually ELVOC? This seems critical for understanding the work.

Response: We thank the reviewer for raising this critical point. The volatility classification, particularly the assignment of certain oxidation products as ELVOCs, indeed has important implications for interpreting their roles in SOA formation and growth processes. In our study, the assignment of compounds to volatility bins (ELVOC, LVOC, SVOC) was based on molecular formulae (see equation (2)). Although our volatility estimates are consistent with current literature and methodology (Schervish and Donahue, 2020), some studies (Stolzenburg et al., 2018; Ye et al., 2018; Schervish and Donahue, 2020) have presented molecular formulas and concentrations of accretion products in different volatility bins. However, the explicit chemical kinetics of the related reactions (such as intermediate products and their yields) are not provided. Therefore, we are unable to accurately represent all of the final products mentioned in these studies within the CAM6-Chem. We acknowledge that this simplification may lead to uncertainty in the volatility of HOMs, and this should be thoroughly discussed. We have added the following discussion at the end of Section 5 (Conclusion):

> *There may be some overestimations of C_{15} and C_{20} if all the accretion products are assumed to be ELVOC or ULVOC. In the updated model, $C_{15}H_{18}O_9$ (C_{15}, extremely low volatility) and $C_{20}H_{32}O_8$ (C_{20}, ultra-low volatility) are used as simplified representatives for all C_{15} and C_{20} dimers. While additional low-volatility dimer species have been detected in chamber experiments (Stolzenburg et al., 2018; Ye et al., 2019; Schervish and Donahue, 2020), these studies did not provide explicit chemical kinetics for the reactions (i.e., intermediate products and their yields), which limits the ability to consider more precise volatility estimates for the accretion products in the model. This uncertainty may influence the contribution of both the accretion products and HOMs-SOA to the overall SOA.*

$$log_{10}C^*(300\ K) = (25 - n_C) \times b_C - (n_o - 3n_N) \times b_O - n_N \times b_N - 2\left[\frac{(n_o-3n_N)\times n_C}{n_C+n_o-3n_N}\right] \times b_{CO} \quad (2)$$

where n_C, n_O, and n_N are the number of carbon, oxygen, and nitrogen atoms; b_C = 0.475; b_O = 0.2; b_N = 2.5; b_{CO} = 0.9.

Comment#5: Finally, If you want to claim "Addressing these gaps requires coordinated laboratory measurements and targeted ambient observations to disentangle competing chemical processes."

Then could you please specifically explain what type of ambient measurement would help in this task. How do you envision one could speciate the corresponding chemicals from the ambient gas-phase.

Response: Regarding specific ambient measurements, we believe that advanced techniques such as high-resolution time-of-flight chemical ionization mass spectrometry (HR-ToF-CIMS) combined with targeted chemical ionization methods will be particularly critical. These approaches enable real-time, highly sensitive detection of trace gases and their oxidation products in the gas phase, thereby facilitating the speciation of relevant compounds in the ambient atmosphere.

However, our current understanding of how to practically implement such measurements in the field, and how to effectively transfer laboratory-derived parameters to ambient observations for optimization, remains limited. Therefore, we can only propose directions from the perspective of model development: on the one hand, field observations are needed to characterize the molecular composition and volatility of accretion products; on the other hand, chamber studies are required to constrain MT-bRO_2 branching ratios. In the future, it may be possible to first obtain key parameters in the laboratory and then progressively refine and apply them under ambient conditions. To emphasize these priorities, we have included a directional statement in the final paragraph of the conclusion:

> *To address persistent gaps between model predictions and observations, field campaigns targeting accretion product speciation and chamber studies that constrain MT-bRO_2 branching ratios are needed.*

Picked up
There's an error: "As the number of oxygen atoms in the functional group increases, the volatility of the organics gradually decreases."

Response: Thank you for your valuable feedback. Considering that this statement could lead to some confusion, we have removed the sentence from the original text.

Please reword (page 3): "but the models still lack fully understand the uncertainties."
Response: We have revised the sentence "but the models still lack fully understanding the uncertainties" to "but the models still lack a full understanding of the uncertainties."

"nitrogen dioxide (NOx)" – nitrogen oxides
NOx is not either of the NO and NO2, it is both. Please clarify the staments claiming NOx can help autoxidation.

Response: Thank you for pointing out the error. Yes, we will correct this mistake throughout the text, replacing most instances of "NOx" with "NO".

Reference

Baker, Y., Kang, S., Wang, H., Wu, R., Xu, J., Zanders, A., He, Q., Hohaus, T., Ziehm, T., Geretti, V., Bannan, T. J., O'Meara, S. P., Voliotis, A., Hallquist, M., McFiggans, G., Zorn, S. R., Wahner, A., and Mentel, T. F.: Impact of HO2⁄RO2 ratio on highly oxygenated α-pinene photooxidation products and secondary organic aerosol formation potential, Atmos. Chem. Phys., 24, 4789–4807, https://doi.org/10.5194/acp-24-4789-2024, 2024.

Berndt, T., Richters, S., Jokinen, T., Hyttinen, N., Kurten, T., Otkjaer, R. V., Kjaergaard, H. G., Stratmann, F., Herrmann, H., Sipila, M., Kulmala, M., and Ehn, M.: Hydroxyl radical-induced formation of highly oxidized organic compounds, Nat Commun, 7, 13677, 10.1038/ncomms13677, 2016.

Bianchi, F., Kurten, T., Riva, M., Mohr, C., Rissanen, M. P., Roldin, P., Berndt, T., Crounse, J. D., Wennberg, P. O., Mentel, T. F., Wildt, J., Junninen, H., Jokinen, T., Kulmala, M., Worsnop, D. R., Thornton, J. A., Donahue, N., Kjaergaard, H. G., and Ehn, M.: Highly Oxygenated Organic Molecules (HOM) from Gas-Phase Autoxidation Involving Peroxy Radicals: A Key Contributor to Atmospheric Aerosol, Chem Rev, 119, 3472-3509, 10.1021/acs.chemrev.8b00395, 2019.

Carlton, A. G., de Gouw, J., Jimenez, J. L., Ambrose, J. L., Attwood, A. R., Brown, S., Baker, K. R., Brock, C., Cohen, R. C., Edgerton, S., Farkas, C. M., Farmer, D., Goldstein, A. H., Gratz, L., Guenther, A., Hunt, S., Jaeglé, L., Jaffe, D. A., Mak, J., McClure, C., Nenes, A., Nguyen, T. K., Pierce, J. R., de Sa, S., Selin, N. E., Shah, V., Shaw, S., Shepson, P. B., Song, S., Stutz, J., Surratt, J. D., Turpin, B. J., Warneke, C., Washenfelder, R. A., Wennberg, P. O., and Zhou, X.: Synthesis of the Southeast Atmosphere Studies: Investigating Fundamental Atmospheric Chemistry Questions, B. Am. Meteorol. Soc., 99, 547–567, https://doi.org/10.1175/BAMS-D-16-0048.1, 2018

Dam, M., Draper, D. C., Marsavin, A., Fry, J. L., and Smith, J. N.: Observations of gas-phase products from the nitrate-radical-initiated oxidation of four monoterpenes, Atmos. Chem. Phys., 22, 9017–9031, https://doi.org/10.5194/acp-22-9017-2022, 2022.

Desai, N. S., Moore, A. C., Mouat, A. P., Liang, Y., Xu, T., Takeuchi, M., Pye, H. O. T., Murphy, B., Bash, J., Pollack, I. B., Peischl, J., Ng, N. L., and Kaiser, J.: Impact of Heatwaves and Declining NOx on Nocturnal Monoterpene Oxidation in the Urban Southeastern United States, Journal of Geophysical Research: Atmospheres, 129, e2024JD041482, https://doi.org/10.1029/2024JD041482, 2024.

Draper, D., Almeida, T. G., Iyer, S., Smith, J. N., Kurtén, T., and Myllys, N.: Unpacking the diversity of monoterpene oxidation pathways via nitrooxy–alkyl radical ring-opening reactions and nitrooxy–alkoxyl radical bond scissions, J. Aerosol Sci., 179, 106379, https://doi.org/10.1016/j.jaerosci.2024.106379, 2024.
Ehn, M., Thornton, J. A., Kleist, E., Sipila, M., Junninen, H., Pullinen, I., Springer, M., Rubach, F., Tillmann, R., Lee, B., Lopez-Hilfiker, F., Andres, S., Acir, I. H., Rissanen, M., Jokinen, T., Schobesberger, S., Kangasluoma, J., Kontkanen, J., Nieminen, T., Kurten, T., Nielsen, L. B., Jorgensen, S., Kjaergaard, H. G., Canagaratna, M., Maso, M. D., Berndt, T., Petaja, T., Wahner, A., Kerminen, V. M., Kulmala, M., Worsnop, D. R., Wildt, J., and Mentel, T. F.: A large source of low-volatility secondary organic aerosol, Nature, 506, 476-479, 10.1038/nature13032, 2014.

Harb, S., Cirtog, M., Alage, S., Cantrell, C., Cazaunau, M., Michoud, V., Pangui, E., Bergé, A., Giorio, C., Battaglia, F., and Picquet-Varrault, B.: HOMs and SOA formation from the oxidation of α- and β-phellandrenes by NO3 radicals, EGUsphere [preprint], https://doi.org/10.5194/egusphere-2024-3419, 2024.

Jokinen, T., Berndt, T., Makkonen, R., Kerminen, V. M., Junninen, H., Paasonen, P., Stratmann, F., Herrmann, H., Guenther, A. B., Worsnop, D. R., Kulmala, M., Ehn, M., and Sipila, M.: Production of extremely low volatile organic compounds from biogenic emissions: Measured yields and atmospheric implications, Proc Natl Acad Sci U S A, 112, 7123-7128, 10.1073/pnas.1423977112, 2015.
Kurten, T., Rissanen, M. P., Mackeprang, K., Thornton, J. A., Hyttinen, N., Jorgensen, S., Ehn, M., and Kjaergaard, H. G.: Computational Study of Hydrogen Shifts and Ring-Opening Mechanisms in alpha-Pinene Ozonolysis Products, J Phys Chem A, 119, 11366-11375, 10.1021/acs.jpca.5b08948, 2015.

Lee, B. H., Iyer, S., Kurtén, T., Varelas, J. G., Luo, J., Thomson, R. J., and Thornton, J. A.: Ring-opening yields and auto-oxidation rates of the resulting peroxy radicals from OH-oxidation of α-pinene and β-pinene, Environmental Science: Atmospheres, 3, 399-407, 10.1039/d2ea00133k, 2023.

Lopez-Hilfiker, F. D., Mohr, C., Ehn, M., Rubach, F., Kleist, E., Wildt, J., Mentel, Th. F., Lutz, A., Hallquist, M., Worsnop, D., and Thornton, J. A.: A novel method for online analysis of gas and particle composition: description and evaluation of a Filter Inlet for Gases and AEROsols (FIGAERO), Atmos. Meas. Tech., 7, 983–1001, https://doi.org/10.5194/amt-7-983-2014, 2014.

Li, D.; Huang, W.; Wang, D.; Wang, M.; Thornton, J. A.; Caudillo, L.; Rorup, B.; Marten, R.; Scholz, W.; Finkenzeller, H.; Marie, G.; Baltensperger, U.; Bell, D. M.; Brasseur, Z.; Curtius, J.; Dada, L.; Duplissy, J.; Gong, X.; Hansel, A.; He, X. C.; Hofbauer, V.; Junninen, H.; Krechmer, J. E.; Kurten, A.; Lamkaddam, H.; Lehtipalo, K.; Lopez, B.; Ma, Y.; Mahfouz, N. G. A.; Manninen, H. E.; Mentler, B.; Perrier, S.; Petaja, T.; Pfeifer, J.; Philippov, M.; Schervish, M.; Schobesberger, S.; Shen, J.; Surdu, M.; Tomaz, S.; Volkamer, R.; Wang, X.; Weber, S. K.; Welti, A.; Worsnop, D. R.; Wu, Y.; Yan, C.; Zauner-Wieczorek, M.; Kulmala, M.; Kirkby, J.; Donahue, N. M.; George, C.; El-Haddad, I.; Bianchi, F.; Riva, M. Nitrate Radicals Suppress Biogenic New Particle Formation from Monoterpene Oxidation. Environ. Sci. Technol. 2024, 58 (3), 1601−1614.

Molteni, U., Simon, M., Heinritzi, M., Hoyle, C. R., Bernham- mer, A.-K., Bianchi, F., Breitenlechner, M., Brilke, S., Dias, A., Duplissy, J., Frege, C., Gordon, H., Heyn, C., Jokinen, T., Kürten, A., Lehtipalo, K., Makhmutov, V., Petäjä, T., Pieber, S. M., Praplan, A. P., Schobesberger, S., Steiner, G., Stozhkov, Y., Tomé, A., Tröstl, J., Wagner, A. C., Wagner, R., Williamson, C., Yan, C., Baltensperger, U., Curtius, J., Donahue, N. M., Hansel, A., Kirkby, J., Kulmala, M., Worsnop, D. R., and Dom- men, J.: Formation of highly-oxygenated organic molecules from α-pinene ozonolysis: chemical characteristics, mechanism and kinetic model development, Earth Space Chem., 3, 873–883, https://doi.org/10.1021/acsearthspacechem.9b00035, 2019.

Moller, K. H., Otkjaer, R. V., Chen, J., and Kjaergaard, H. G.: Double Bonds Are Key to Fast Unimolecular Reactivity in First-Generation Monoterpene Hydroxy Peroxy Radicals, J Phys Chem A, 124, 2885-2896, 10.1021/acs.jpca.0c01079, 2020.

Murphy, S. E., Crounse, J. D., Møller, K. H., Rezgui, S. P., Hafeman, N. J., Park, J., Kjaergaard, H. G., Stoltz, B. M., and Wennberg, P. O.: Accretion product formation in the selfreaction of ethene-derived hydroxy peroxy radicals, Environ. Sci.-Atmos., 3, 882–893, https://doi.org/10.1039/D3EA00020F, 2023.

Nah, T., Sanchez, J., Boyd, C. M., and Ng, N. L.: Photochemical Aging of α-pinene and β-pinene Secondary Organic Aerosol formed from Nitrate Radical Oxidation, Environ. Sci. Technol., 50, 222-231, 10.1021/acs.est.5b04594, 2016.

Pasik, D., Golin Almeida, T., Ahongshangbam, E., Iyer, S., and Myllys, N.: Monoterpene oxidation pathways initiated by acyl peroxy radical addition, Atmos. Chem. Phys., 25, 4313–4331, https://doi.org/10.5194/acp-25-4313-2025, 2025.

Pye, H. O. T., D'Ambro, E. L., Lee, B. H., Schobesberger, S., Takeuchi, M., Zhao, Y., Lopez-Hilfiker, F., Liu, J., Shilling, J. E., Xing, J., Mathur, R., Middlebrook, A. M., Liao, J., Welti, A., Graus, M., Warneke, C., de Gouw, J. A., Holloway, J. S., Ryerson, T. B., Pollack, I. B., and Thornton, J. A.: Anthropogenic enhancements to production of highly oxygenated molecules from autoxidation, Proc Natl Acad Sci U S A, 116, 6641-6646, 10.1073/pnas.1810774116, 2019.

Richters, S., Herrmann, H., and Berndt, T.: Highly Oxidized RO2 Radicals and Consecutive Products from the Ozonolysis of Three Sesquiterpenes, Environ Sci Technol, 50, 2354-2362, 10.1021/acs.est.5b05321, 2016.

Rissanen, M. P., Kurtén, T., Sipilä, M., Thornton, J. A., Kausiala, O., Garmash, O., Kjaergaard, H. G., Petäjä, T., Worsnop, D. R., Ehn, M., and Kulmala, M.: Effects of Chemical Complexity on the Autoxidation Mechanisms of Endocyclic Alkene Ozonolysis Products: From Methylcyclohexenes toward Understanding á-Pinene, J. Phys. Chem. A, 119, 4633–4650, https://doi.org/10.1021/jp510966g, 2015.

Roldin, P., Ehn, M., Kurten, T., Olenius, T., Rissanen, M. P., Sarnela, N., Elm, J., Rantala, P., Hao, L., Hyttinen, N., Heikkinen, L., Worsnop, D. R., Pichelstorfer, L., Xavier, C., Clusius, P., Ostrom, E., Petaja, T., Kulmala, M., Vehkamaki, H., Virtanen, A., Riipinen, I., and Boy, M.: The role of highly oxygenated organic molecules in the Boreal aerosol-cloud-climate system, Nat Commun, 10, 4370, 10.1038/s41467-019-12338-8, 2019.

Rolletter, M., Kaminski, M., Acir, I. H., Bohn, B., Dorn, H. P., Li, X., Lutz, A., Nehr, S., Rohrer, F., Tillmann, R., Wegener, R., Hofzumahaus, A., Kiendler-Scharr, A., Wahner, A., and Fuchs, H.: Investigation of the α-pinene photooxidation by OH in the atmospheric simulation chamber SAPHIR, Atmos. Chem. Phys., 19, 11635-11649, 10.5194/acp-19-11635-2019, 2019.

Saunders, S. M., Jenkin, M. E., Derwent, R. G., and Pilling, M. J.: Protocol for the development of the Master Chemical Mechanism, MCM v3 (Part A): tropospheric degradation of non-aromatic volatile organic compounds, Atmos. Chem. Phys., 3, 161-180, 10.5194/acp-3-161-2003, 2003.

Schervish, M. and Donahue, N. M.: Peroxy radical chemistry and the volatility basis set, Atmos. Chem. Phys., 20, 1183–1199, https://doi.org/10.5194/acp-20-1183-2020, 2020.

Stolzenburg, D., Fischer, L., Vogel, A. L., Heinritzi, M., Schervish, M., Simon, M., Wagner, A. C., Dada, L., Ahonen, L. R., Amorim, A., Baccarini, A., Bauer, P. S., Baumgartner, B., Bergen, A., Bianchi, F., Breitenlechner, M., Brilke, S., Buenrostro Mazon, S., Chen, D., Dias, A., Draper, D. C., Duplissy, J., El Haddad, I., Finkenzeller, H., Frege, C., Fuchs, C., Garmash, O., Gordon, H., He, X., Helm, J., Hofbauer, V., Hoyle, C. R., Kim, C., Kirkby, J., Kontkanen, J., Kürten, A., Lampilahti, J., Lawler, M., Lehtipalo, K., Leiminger, M., Mai, H., Mathot, S., Mentler, B., Molteni, U., Nie, W., Nieminen, T., Nowak, J. B., Ojdanic, A., Onnela, A., Passananti, M., Petäjä, T., Quéléver, L. L. J., Rissanen, M. P., Sarnela, N., Schallhart, S., Tauber, C., Tomé, A., Wagner, R., Wang, M., Weitz, L., Wimmer, D., Xiao, M., Yan, C., Ye, P., Zha, Q., Baltensperger, U., Curtius, J., Dommen, J., Flagan, R. C., Kulmala, M., Smith, J. N., Worsnop, D. R., Hansel, A., Donahue, N. M., and Winkler, P. M.: Rapid growth of organic aerosol nanoparticles over a wide tropospheric temperature range, P. Natl. Acad. Sci. USA, 115, 9122–9127, https://doi.org/10.1073/pnas.1807604115, 2018.

Weber, J., Archer-Nicholls, S., Griffiths, P., Berndt, T., Jenkin, M., Gordon, H., Knote, C., and Archibald, A. T.: CRI-HOM: A novel chemical mechanism for simulating highly oxygenated organic molecules (HOMs) in global chemistry–aerosol–climate models, Atmos. Chem. Phys., 20, 10889-10910, 10.5194/acp-20-10889-2020, 2020.

Xu, L., Moller, K. H., Crounse, J. D., Otkjaer, R. V., Kjaergaard, H. G., and Wennberg, P. O.: Unimolecular Reactions of Peroxy Radicals Formed in the Oxidation of alpha-Pinene and beta-Pinene by Hydroxyl Radicals, J Phys Chem A, 123, 1661-1674, 10.1021/acs.jpca.8b11726, 2019.
Yan, C., Nie, W., Äijälä, M., Rissanen, M. P., Canagaratna, M. R., Massoli, P., Junninen, H., Jokinen, T., Sarnela, N., Häme, S. A. K., Schobesberger, S., Canonaco, F., Yao, L., Prévôt, A. S. H., Petäjä, T., Kulmala, M., Sipilä, M., Worsnop, D. R., and Ehn, M.: Source characterization of highly oxidized multifunctional compounds in a boreal forest environment using positive matrix factorization, Atmos. Chem. Phys., 16, 12715-12731, 10.5194/acp-16-12715-2016, 2016.

Schervish, M. and Donahue, N. M.: Peroxy radical chemistry and the volatility basis set, Atmospheric Chemistry and Physics, 20, 1183-1199, 10.5194/acp-20-1183-2020, 2020.

Stolzenburg, D., Fischer, L., Vogel, A. L., Heinritzi, M., Schervish, M., Simon, M., Wagner, A. C., Dada, L., Ahonen, L. R., Amorim, A., Baccarini, A., Bauer, P. S., Baumgartner, B., Bergen, A., Bianchi, F., Breitenlechner, M., Brilke, S., Buenrostro Mazon, S., Chen, D., Dias, A., Draper, D. C., Duplissy, J., El Haddad, I., Finkenzeller, H., Frege, C., Fuchs, C., Garmash, O., Gordon, H., He, X., Helm, J., Hofbauer, V., Hoyle, C. R., Kim, C., Kirkby, J., Kontkanen, J., Kürten, A., Lampilahti, J., Lawler, M., Lehtipalo, K., Leiminger, M., Mai, H., Mathot, S., Mentler, B., Molteni, U., Nie, W., Nieminen, T., Nowak, J. B., Ojdanic, A., Onnela, A., Passananti, M., Petäjä, T., Quéléver, L. L. J., Rissanen, M. P., Sarnela, N., Schallhart, S., Tauber, C., Tomé, A., Wagner, R., Wang, M., Weitz, L., Wimmer, D., Xiao, M., Yan, C., Ye, P., Zha, Q., Baltensperger, U., Curtius, J., Dommen, J., Flagan, R. C., Kulmala, M., Smith, J. N., Worsnop, D. R., Hansel, A., Donahue, N. M., and Winkler, P. M.: Rapid growth of organic aerosol nanoparticles over a wide tropospheric temperature range, P. Natl. Acad. Sci. USA, 115, 9122-9127, 10.1073/pnas.1807604115, 2018.

Xu, R. C., Thornton, J. A., Lee, B., Zhang, Y. X., Jaegle, L., Lopez-Hilfiker, F. D., Rantala, P., and Petaja, T.: Global simulations of monoterpene-derived peroxy radical fates and the distributions of highly

oxygenated organic molecules (HOMs) and accretion products, Atmos. Chem. Phys., 22, 5477-5494, 10.5194/acp-22-5477-2022, 2022.

Ye, Q., Wang, M., Hofbauer, V., Stolzenburg, D., Chen, D., Schervish, M., Vogel, A., Mauldin, R. L., Baalbaki, R., Brilke, S., Dada, L., Dias, A., Duplissy, J., El Haddad, I., Finkenzeller, H., Fischer, L., He, X., Kim, C., Kürten, A., Lamkaddam, H., Lee, C. P., Lehtipalo, K., Leiminger, M., Manninen, H. E., Marten, R., Mentler, B., Partoll, E., Petäjä, T., Rissanen, M., Schobesberger, S., Schuchmann, S., Simon, M., Tham, Y. J., Vazquez-Pufleau, M., Wagner, A. C., Wang, Y., Wu, Y., Xiao, M., Baltensperger, U., Curtius, J., Flagan, R., Kirkby, J., Kulmala, M., Volkamer, R., Winkler, P. M., Worsnop, D., and Donahue, N. M.: Molecular Composition and Volatility of Nucleated Particles from á-Pinene Oxidation between −50 °C and +25 °C, Environ. Sci. Technol., 53, 12357–12365, https://doi.org/10.1021/acs.est.9b03265, 2019.

Zawadowicz, M. A., Lee, B. H., Shrivastava, M., Zelenyuk, A., Zaveri, R. A., Flynn, C., Thornton, J. A., and Shilling, J. E.: Photolysis Controls Atmospheric Budgets of Biogenic Secondary Organic Aerosol, Environ. Sci. Technol., 54, 3861-3870, 10.1021/acs.est.9b07051, 2020.

Zhao, Y., Thornton, J. A., and Pye, H. O. T.: Quantitative constraints on autoxidation and dimer formation from direct probing of monoterpene-derived peroxy radical chemistry, Proc Natl Acad Sci U S A, 115, 12142-12147, 10.1073/pnas.1812147115, 2018.

Zhao, Y., Saleh, R., Saliba, G., Presto, A. A., Gordon, T. D., Drozd, G. T., Goldstein, A. H., Donahue, N. M., and Robinson, A. L.: Reducing secondary organic aerosol formation from gaso- line vehicle exhaust, P. Natl. Acad. Sci. USA, 114, 6984–6989, https://doi.org/10.1073/pnas.1620911114,, 2017.